Bulletin of Volcanology (2025) 87:126
https://doi.org/10.1007/s00445-025-01908-y

RESEARCH ARTICLE

Probabilistic volcanic hazard assessment during quiescence: A scenario-based approach for Gede, West Java (Indonesia)

Eleanor Tennant[1] · Susanna F. Jenkins[1] · Annie Winson[2] · Christina Widiwijayanti[1] · Heruningtyas D. Purnamasari[3] · Nugraha Kartadinata[3] · Wilfridus Banggur[4]

Received: 25 February 2025 / Accepted: 25 October 2025 / Published online: 3 December 2025

Abstract

One of the first steps towards reducing volcanic risk is assessing the area likely to be affected by hazardous phenomena. This typically involves analysis of a volcano's past eruptions to forecast the expected size and style of future eruptions and the spatial extent of the expected hazards. However, there are many active volcanoes worldwide that do not have extensive eruption records from which to forecast future behaviours; Gede volcano in Indonesia is one example. In this work, we conducted the first probabilistic volcanic multi-hazard assessment for five different hazards from six eruptive scenarios for Gede, the closest active volcano to Jakarta city. To supplement Gede's eruption record, we used analogue volcanoes and global datasets to develop eruption scenarios and to parameterise hazard models. Our analysis suggests that the major explosive eruption scenario and the Plinian explosive eruption scenario, which have column heights of 10–20 km and 20–30 km respectively, can deposit sufficient tephra to disrupt airport operations and vital lifelines across Jakarta, while tephra fall from the continuously explosive or intermittently explosive eruption scenarios may obscure road markings and disrupt agricultural operations proximal to the volcano. Hazards from effusive scenarios primarily impact the volcano's northeastern flank; lava flows are confined to ~ 3 km in this direction while block-and-ash flows are expected to extend up to ~ 11 km. Pyroclastic density currents from a collapsing column from the minor explosive eruption scenario (column height 1–10 km) can extend up to ~ 15 km but could reach up to ~ 20–25 km for major and Plinian eruption scenarios. Through this work, we provide a probabilistic hazard assessment for Gede and a framework for volcanic hazard assessment in data-limited contexts. This assessment serves as an essential tool for enhancing risk mitigation through planning and preparedness in one of the most exposed regions of the world.

Keywords Volcanic hazard assessment · Probabilistic hazard · Multi-hazard · Data-limited

Introduction

Disaster preparedness is a fundamental element of disaster risk reduction (UNISDR, 2005; 2015). For volcanic hazards, as with other natural hazards, the first step in preparedness is to understand the phenomena, their destructive effects, and their expected spatial extent. This understanding is formalised through long-term volcanic hazard assessment that involves gathering information about past eruptions using geological studies and/or historical reports. The collected data can be used to develop scenarios that describe expected future eruptions and to model the spatial extent of associated hazards within a forecasting time window of years to decades (Marzocchi and Bebbington 2012). These hazard assessments serve as the backbone for the development of emergency management strategies, hazard awareness

Editorial responsibility: P. Tierz

✉ Eleanor Tennant
eleanorm001@e.ntu.edu.sg

[1] Earth Observatory of Singapore and Asian School of the Environment, Nanyang Technological University, Singapore 639798, Singapore

[2] British Geological Survey, Keyworth, Nottingham NG12 5GG, United Kingdom

[3] Center for Volcanology and Geological Hazard Mitigation, Bandung City, West Java 40122, Indonesia

[4] National Research and Innovation Agency, Jakarta 10340, Indonesia

education, and land-use management practices (Hayes et al. 2020; Martí et al. 2022). Furthermore, given renewed unrest at a volcano, long-term analyses act as foundational knowledge that can be drawn from and interpreted in light of monitoring data to produce short-term hazard forecasts (Marzocchi et al. 2004, 2008; Sandri et al. 2012).

Probabilistic frameworks have become the benchmark in volcanic hazard assessment, allowing for the quantification of both aleatory and epistemic uncertainty (Tierz 2020). When it comes to modelling the spatial extent of volcanic hazards, this uncertainty quantification is accounted for by sampling from distributions of model input parameters such that a wide range of possible credible combinations is simulated. Within existing probabilistic hazard assessment studies, a variety of approaches exist in terms of:

1) The way that scenarios are defined and the number of scenarios that are included. Some studies focus on eruption size described by the VEI (e.g., Sandri et al. 2014; Jiménez et al. 2020; Alcozer-Vargas et al. 2022; Warwick et al. 2022), while others categorise scenarios based on eruption style (e.g., Weir et al. 2022; Aravena et al. 2023; Tadini et al., 2025). The number of scenarios that are considered generally ranges from 1–4, and the choice of scenarios is usually based on past eruptions.
2) The number of hazards that are considered, with studies conducted for single (e.g., Sandri et al. 2018; Clarke et al. 2020; Lombardi et al. 2020) or multiple hazards (e.g., Becerril et al. 2014; Sandri et al. 2014; Tierz et al. 2017; Jiménez et al. 2020; Reyes-Hardy et al. 2021; Alcozer-Vargas et al. 2022; Bertin et al. 2022; Constantinescu et al. 2022; Mead et al. 2022; Weir et al. 2022; Aravena et al. 2023).
3) The inclusion or absence of temporal analyses. For hazard assessments at volcanoes with extensive eruption records, long-term eruption recurrence rates have been quantified by dividing the record length by the number of recorded eruptions (e.g., Becerril et al. 2014). This approach can then be extended to calculate a frequency-magnitude relationship for a particular volcano. However, there is considerable uncertainty in deriving frequency-magnitude relationships for volcanoes with limited eruption records (Hayes et al. 2022), and most published hazard maps are conditional on the occurrence of an eruption of a specific size and/or style (Lindsay et al. 2023).
4) The application of more advanced statistical techniques for hazard assessment such as the incorporation of Bayesian statistics (e.g., Becerril et al. 2014; Sandri et al. 2014; Bartolini et al. 2015; Constantinescu et al. 2022), which may be facilitated by software packages such as HASSET (Sobradelo et al. 2014) and BET_VH (Marzocchi et al. 2010), or Bayesian belief networks (e.g., Hincks et al. 2014; Tierz et al. 2017) or the inclusion of statistical emulators (e.g., Bayarri et al. 2009; Spiller et al. 2014; Tierz et al. 2024).

Understandably, hazard assessments are often conducted for frequently active, well-known volcanoes. However, there are many volcanoes across the world that remain data-limited (Loughlin et al. 2015). This can be due to long recurrence intervals between eruptions, insufficient deposit preservation or study, and/or differences in eruption recording across the world. With limited information available for forecasting, assessing the expected future hazards at these volcanoes requires the identification and use of information from carefully selected analogous volcanoes (Tierz et al. 2019; Burgos et al. 2023), global datasets (Tierz 2020), or the use of expert elicitation (Jenkins et al. 2024a). With 23 recorded eruptions since 1747 CE, and a large gap between these historic eruptions and the eruptions preserved in the geological record, Gede volcano in west Java, Indonesia, is a potentially dangerous, active volcano that poses a challenge to robust forecasting of future activity. Due to its proximity to Indonesia's highly populated city of Jakarta (~ 11.4 million people, World Population Review, 2024), Gede has the highest number of people living within 100 km out of any volcano in the world (Small and Naumann 2001). Closer to the volcano, the number of people is more modest, but when population exposure is weighted by distance, Gede has the third highest population exposure index (PEI) out of Holocene volcanoes in southeast Asia (Jenkins et al. 2022).

Despite Gede's high-threat status, to our knowledge there have been just a handful of published works that focus on the volcano. Field studies conducted by the Volcanological Survey of Indonesia (now known as the Center for Volcanology and Geological Hazard Mitigation – CVGHM) in 1992 were used to compile the official hazard map for Gede (Hadisantono et al. 2008) (shapefiles available at: https://vsi.esdm.go.id/portalmbg/). The hazard map is deterministic, delineating hazard zones (1, 2, 3) that group multiple hazards, and is based on the occurrence of a small vulcanian-style eruption (Hadisantono et al. 2008). Since then, geochemical studies have been conducted by Handley et al. (2010), Belousov et al. (2015), and Krimer (2016). Bear-Crozier et al. (2012) considered tephra fall hazard from a single set of eruption parameters under a suite of atmospheric conditions, while Winson (2016) generated probabilistic tephra fall simulations for various VEI scenarios. Tennant et al. (2021) aimed to reconstruct past eruptions at Gede using numerical hazard models Titan2D and Tephra2 to better understand the dynamics of eruptions that produced the PDC deposits observed in the field and tephra fall that was reported in Jakarta.

In this work, we build on these previous studies by consolidating all available information on past eruptions at

Gede and using this to conduct the first probabilistic volcanic hazard assessment for five different hazards at Gede. We expanded the limited dataset of Gede's past eruptions with data from analogous volcanoes and global datasets. This allowed us to outline a series of potential eruption scenarios and model the spatial extent of the associated hazards. Our assessment considers the hazard from tephra fall, large clasts (large lapilli sized particles, 16–64 mm diameter), column collapse style pyroclastic density currents (PDCs), block-and-ash flows, and lava flows. This study serves as a case example for conducting hazard assessments on volcanoes where eruption records are lacking in detail or quantity and lays the groundwork for future risk analyses and disaster preparedness strategies at Gede.

Geological background and eruptive history

Gede is an active stratovolcano (2958 m asl) situated within the Sunda arc, which delineates the northeastwards subduction of the Indo-Australian plate beneath the Eurasian plate. The volcano consists of a main stratocone known as Gumuruh or 'old Gede' that is comprised of silica-rich basalt. Gumuruh grew and collapsed during the Pleistocene leaving a 10 km^3 debris avalanche deposit that underlies Cianjur

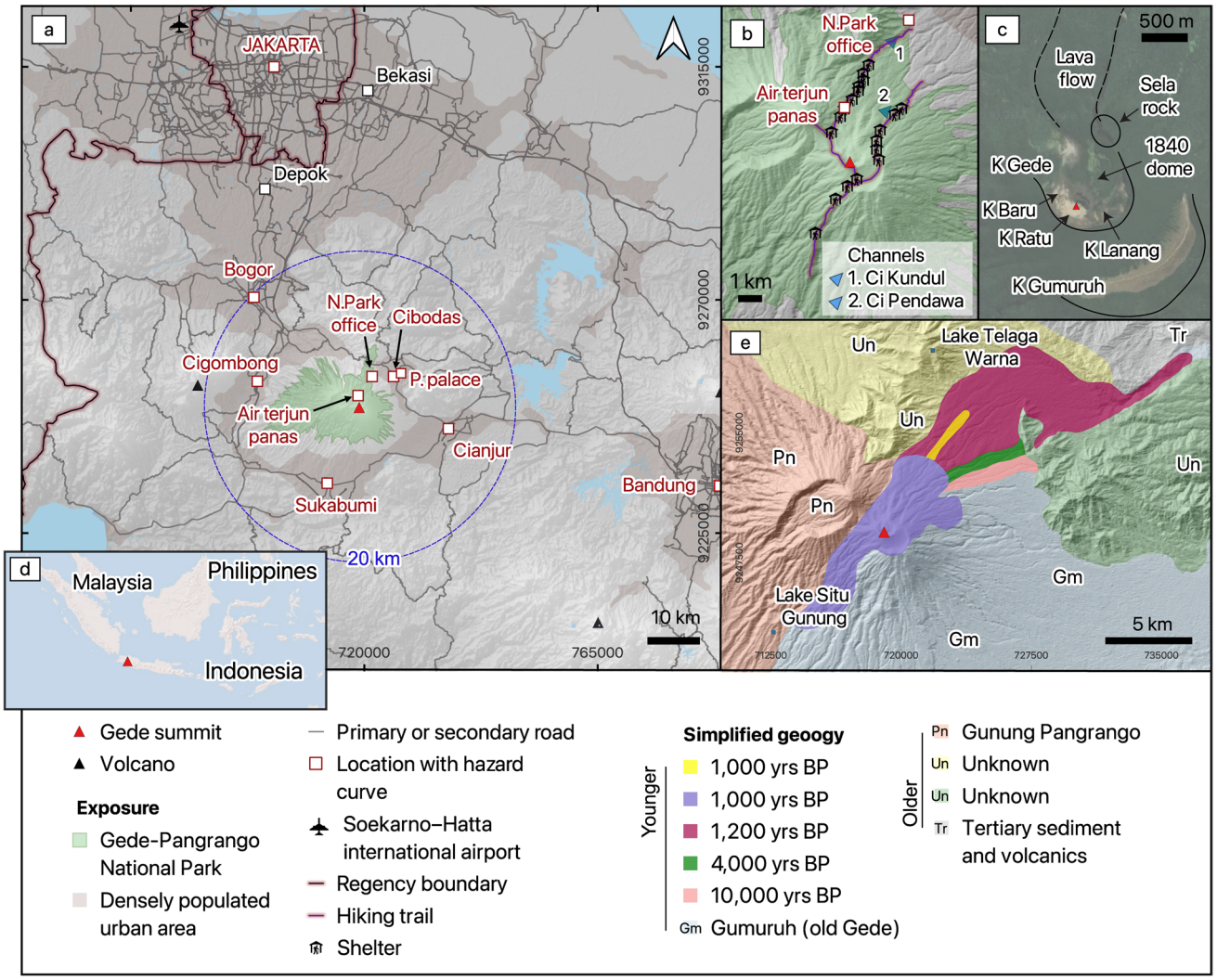

Fig. 1 **a** The location of Gede showing its proximity to Jakarta and other densely populated urban areas; the blue circle marks a 20 km radial distance from the summit for reference; **b** The topography of the summit area and the locations of the hiking trails and shelters; **c** The summit of Gede showing topographic features including past craters (Kawah [K] in Indonesian); **d** The location of Gede within Southeast Asia; **e** A simplified geological map of Gede showing Holocene (brighter colours) and older deposits (muted colours), adapted from Belousov et al. (2016) and the official geological map of Gede (Hadisantono et al. 2008). Spatial data showing densely populated urban areas is from the Global Human Settlement layer (Pesaresi and Panagiotis 2023), and the locations of roads, towns and cities are from Open Street Map (OSM). For all maps: the coordinate reference system is EPSG: 32748, basemap credit: ESRI shaded relief

town in the southeast (Belousov et al. 2015) (Fig. 1). The cone was later rebuilt, to form the present-day intra-caldera cone of Gede. During the Holocene, Gede exhibited predominantly explosive eruptions, ranging from VEI 1 to 4. Holocene eruptions generated flow deposits extending up to 15 km away from the summit dated at 10,000, 4,000, 1,200, and 1,000 years before present (BP) (Belousov et al. 2015). Deposits are primarily found in the northeast sector of the volcano due to the topographic constrains imposed by a northerly breach in the Gede crater wall and the presence of Gede's twin, long-dormant volcano Pangrango (Fig. 1b).

During historic times (since 1747), Gede has experienced 23 eruptions (1747, 1761, 1832, 1840, 1843, 1845, 1847, 1848, 1852, 1853, 1866, 1870, 1887, 1888, 1891, 1899, 1900, 1909, 1946, 1947, 1948, 1949, 1957 [phreatic]). Except for one VEI 1 eruption (1909) and four VEI 3 eruptions (1747, 1832, 1840, and 1853), these were all assigned a VEI 2. In the Global Volcanism Program, this is the default assignation for eruptions that were explosive but lack detailed information (Siebert et al., 2011). As a result, there is some uncertainty about whether all VEI 2 assigned eruptions were of that size. Historic eruptions at Gede have been described by Junghuhn (1853); Kusumadinata (1979); Newmann van Padang (1951); NTNI (1852, 1859, 1871, 1886, 1887, 1889, 1890, 1891, 1900, 1902, 1924); Petroeschevsky (1943, 1952); many of these accounts of earlier eruptions consist of qualitative descriptions that are challenging to infer eruption size or style from. The later accounts (post 1900) provide more detail and suggest that eruptions were dominantly explosive, vulcanian type, with reported plume heights of up to 5 km above the vent (see Tennant et al. 2021 Appendices A and B for a compiled eruption history). The extent of tephra fall produced during historic times is uncertain. During field studies, Belousov et al. (2015) found no recent tephra fall outside of the proximal ring plain, while a written account of the 1948 eruption (Petroeschevsky 1952) suggested that fallout was reported in Jakarta, which was not reproducible using numerical modelling of the event and wind conditions (ECMWF ERA20C) at the time of the eruption (Tennant et al. 2021). During the 1840 eruption, the crater of Gede was filled with a blocky andesitic lava dome, which breached the crater towards the northeast to form a 1.5 km lava flow (Fig. 1c). Today, there is persistent fumarolic activity at the summit and since the installation of seismometers by CVGHM in 1985, seismic swarms have been recorded every 1–2 years (Hidayat et al. 2019).

Exposure

The area surrounding Gede has a permanent population of ~ 440,000 people within 10 km of the summit (Schiavina et al. 2023). The flanks of the volcano are heavily farmed, and approximately 70% of this permanent population works in agriculture (Nurwulan 2016), cultivating tea, rice, vegetables, and other crops (Tang et al. 2024). In addition to the permanent population, Gede is situated within the Gede-Pangrango national park, in an area of high biodiversity that attracts both geo- and eco-tourists from the nearby cities of Jakarta (60 km northwest), Bogor (28 km northwest, population: ~ 800,000, World Population Review, 2024), and Sukabumi (15 km southwest, population: ~ 270,000, World Population Review, 2024) amongst other locations. The park receives > 70,000 visitors annually (Nurwulan 2016), many of whom hike to the peaks of Gede and/or Pangrango via the northeast trail located within the Ci Kundul river channel (Fig. 1c), often choosing to camp at the summit area. The national park office, located within Cibodas town ~ 7 km to the northeast, is the starting point for hikers and a hub for tourist activities. Cibodas is a popular choice for second homeowners who reside in the local cities and is the site of the Cipanas presidential palace, a place of cultural significance.

Defining eruption scenarios

Choosing analogue volcanoes

Given the limited eruption record of Gede, we used analogue volcanoes to help define eruption scenarios and to parameterise hazard model inputs. The choice of analogue volcanoes is often based on expert judgement (e.g., Aspinall et al. 2003; Hincks et al. 2014; Bebbington et al. 2018) and/or qualitative grouping of volcanoes based on: volcano type, tectonic setting, morphology, and eruption style. However, recent approaches have been developed to provide a quantitative and transparent basis for considering volcanoes analogous (e.g., Tierz et al. 2019; Burgos et al. 2023). To develop a set of analogue volcanoes for Gede, we compared the results from three different analogue selection methods: one semi-quantitative (Whelley et al. 2015) and two quantitative methods (Tierz et al. 2019; Burgos et al. 2023. Whelley et al. (2015) classified volcanoes based on their capacity for shallow or deep buffering of intruded magma using proxies such as petrological indicators, the size of the largest recorded eruption, and volcano morphology. Tierz et al. (2019) used GVP and volcano-morphology data (Pike and Clow, 1981; Grosse et al. 2014) in a method (VOLCANS) that allows users to weigh different volcanological criteria to calculate volcano analogy between any volcano listed in GVP (currently, the method is openly available through the Python package, PyVOLCANS, Tierz et al. 2021). Burgos et al. (2023) used similar but expanded datasets (e.g., magma-geochemistry or tectonic-setting parameters) in a hierarchical clustering approach that made use of 38

numerical variables to group volcanoes. To qualify as a suitable analogue for Gede, we determined that a volcano should be classified as a stratovolcano by the Global Volcanism Program (GVP), appear in at least two of the three analogue set lists, and have a history of vulcanian-style eruptions in its record (at least one). These criteria produced an analogue set of 23 volcanoes located in Indonesia: Kerinci, Lewotobi, Papandayan, Salak, Sumbing, Bur Ni Telong; Russia: Alaid, Avanchinsky, Etorofu-Atosanupuri, Fuss Peak, Karymsky, Kharimkotan, Koryaksky, Sinarka; Chile: Lautaro, San Jose, Tupungatito; Colombia: Cumbal, Purace; USA: Chiginagak, Redoubt; Papua New Guinea: Bam; and Peru: Sabancaya.

Scenarios considered

Volcanic eruptions are complex, multi-phase events, where phases exhibit distinct characteristics and pose unique hazards over different timescales. Recognizing this variability and the need for increased granularity in hazard assessments to support emergency management (Tierz 2020), in our assessment we evaluated the hazards associated with different eruption phases. Bebbington and Jenkins (2019) disaggregated the eruptions present in the GVP database into eruptive phases, of which some are prolonged (durations > 1 day): effusive activity (*Eff*), continuously explosive activity (*Cont-exp*), intermittently explosive (*Int-exp*); and some are discrete (durations < 1 day): minor (*Min-exp*), major (*Maj-exp*), or Plinian explosive (*Plin-exp*) eruption (Bebbington and Jenkins 2019, 2022) (Table 1). The study also identified three additional phases, a deformation phase, a combined effusive-explosive phase, and a minor explosion phase, that were excluded from our analysis for Gede. The minor explosion phase, characterised by a single explosion of the intermittently explosive style, was not observed in past eruptions at these volcanoes and was absent from the Gede plus analogues dataset. The deformation phase occurred only once in the dataset and was disregarded since it does not correspond to eruptive activity. Hazards from the combined effusive-explosive phase were assumed to be similar to those from individual effusive or intermittently explosive pulses and were not modelled separately.

We examined the phase sequences from the Bebbington and Jenkins (2022) dataset combining the seven records from Gede's eruption history that were present in the dataset with 101 records from the 16 analogue volcanoes available to understand the potential sequences for eruptions at Gede. Analogue volcanoes that were not included in the Bebbington and Jenkins (2022) dataset are: Cumbal (Colombia), Etorofu-Atosanupuri (Russia), Fuss Peak (Russia), Salak (Indonesia), San Jose (Chile), Sumbing (Indonesia), Telong Bur ni (Indonesia). The combined Gede plus analogues dataset consisted of 108 eruptions with 336 phases (Online Resource 1). Of these eruptions, 40% were single phase and 60% were multiphase (Fig. 2). For single phase eruptions, activity was typically short lived, with 79% of the single-phase dataset being of 1 day duration or less. The maximum duration of a single phase eruption was 729 days (Papandayan, Indonesia [1923–1925]). The most common single phase was the *Min-exp* phase (22% of all eruptions) followed by the *Int-exp* phase (12% of all eruptions). For multiphase eruptions, the majority (39%) contained two non-quiescent phases. The most common (44%) progression of phases was *Min-exp* followed by quiescence and then another *Min-exp* phase. Phase durations were longer than in single phase eruptions (Fig. 2), and total duration for the multiphase eruptions was between 2 and 4513 days (> 12 years) (Karymsky, Russia [1970–1982]).

These statistics show that while nearly two thirds of eruptions at Gede and its analogues contain 1 or 2 phases, there have been eruptions with as many as 15 distinct phases of activity. Given the practical challenges of modelling all 54 unique sequences present in the dataset and recognising

Table 1 Hazards assigned to each of the eruption phases from Bebbington and Jenkins., 2019, that are considered likely at Gede. Prolonged phases have durations > 1 day, while discrete phases last for 1 day or less

	Scenario ID	Description	Notes	Hazards
Prolonged phases	*Eff*	Effusive	Solely effusive activity: extrusion of lava domes, flows, and fountains	Lava flows, PDC- BAF
	Cont-exp	Continuously explosive	Explosive activity described as continuous or Strombolian	Tephra fall, large clasts
	Int-exp	Intermittently explosive	Explosive activity described as intermittent or Vulcanian, or with a date range exceeding 2 days without mention of a major explosion	Tephra fall, large clasts
Discrete phases	*Min-exp*	Minor explosive	c. < 10 km column height	Tephra fall, large clasts, PDC-CC
	Maj-exp	Major explosive	c. 10–20 km column height. Many VEI 3 and most VEI 4 eruptions will have at least one	Tephra fall, large clasts, PDC-CC
	Plin-exp	Plinian explosive	c. > 20 km column height. Most VEI 5 and all VEI 6 + eruptions will have at least one	Tephra fall, large clasts, PDC-CC

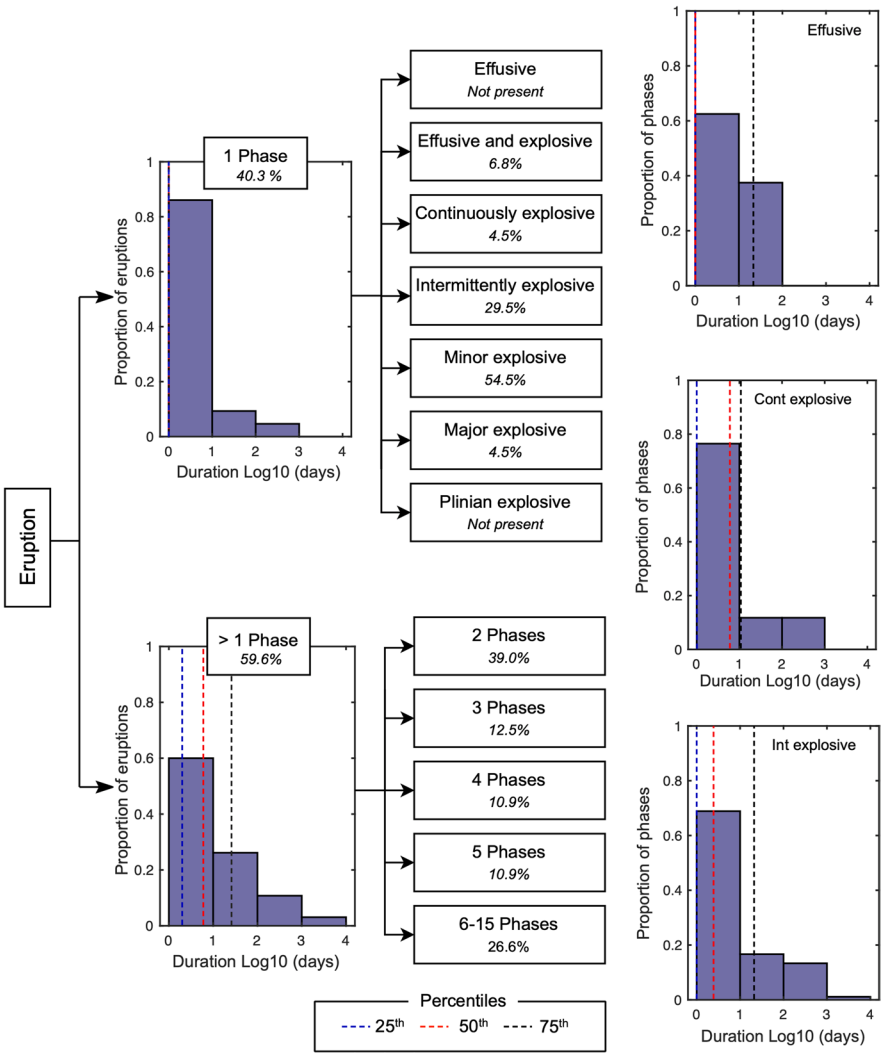

Fig. 2 Schematic showing the proportions (%) of the different phase sequences in the combined Gede plus analogue eruption records extracted from the Bebbington and Jenkins, (2022) phases dataset along with the durations of single and multi-phase eruptions and, prolonged phases (effusive [Eff], continuously explosive [Cont-exp], and intermittently explosive [Int-exp]). Dashed lines in the duration plots represent the 25th, 50th and 75th percentiles. Note that in the 1 phase plot lines for the 25th, 50th and 75th percentiles are overlapping and in the Effusive plot lines for the 25th and 50th percentiles are overlapping

that over 50% of eruptions in the analogue dataset involve either a single phase or consecutive phases of the same type, we chose to focus on single-phase eruptions. Nevertheless, we note that to produce hazard footprints associated with multi-phase eruptions, where there are limited changes to the topography or tephra deposit clean-up operations conducted, single-phase footprints may be aggregated for some hazards. Alternatively, where the first phase results in changes to the topography, multi-phase eruptions may be modelled using our single-phase scenarios as a starting point and adapting the topography between phases (e.g., Weir et al. 2022). For simplicity, from here on in we refer to the eruption phases presented in Table 1 as scenarios.

For each eruption scenario, we assigned the likely hazards (Table 1) and interrogated bulletin reports from the Global Volcanism Program (https://volcano.si.edu/) along with available published literature pertaining to our analogue volcanoes for model input parameters (e.g., column heights, erupted volumes). In the section that follows, we describe the hazard models and the input parameters used for analysis.

Modelling volcanic hazards

We modelled five primary hazards that are possible at Gede: tephra fall, large clasts, lava flows, and PDCs generated by two different mechanisms: the collapse of a vertical eruptive column and the gravitational collapse of a lava dome (block-and-ash flows, BAF). Large clasts refer to coarse lapilli-sized particles (16–64 mm) that sediment from the margins of the eruption column. Their transport behaviour is intermediate between wind-advected and purely ballistic trajectories (Rossi et al. 2019), which is not captured by models developed for tephra fall or ballistic projectiles. Ballistic projectiles often fall within 5 km of the vent, though

they can extend up to 10 km away (Fitzgerald et al. 2014; Bertin 2017). Large clasts can travel further than this and fall with impact energies sufficient to cause harm to people and infrastructure (e.g., Osman et al. 2019). For small explosive eruptions such as lava fountains or small vulcanian-style eruptions where ballistics often fall within 1–2 km from the vent (Calvari and Pinkerton 2002), large clasts can fall out more than 10 km away (Andronico et al. 2015).

For all hazards, the hazard models used in this study were chosen for their applicability in a probabilistic context, which requires sufficiently rapid computational times to allow for many thousands of simulations. In the sections that follow, we describe the main inputs used for hazard models; tables describing the full inputs can be found in Online Resources 2–6. The outputs produced by the different hazard models and their use in the preparation of visual hazard outputs are described in Sect. "Preparation of hazard outputs and hazard intensity thresholds".

Tephra fall

To identify the area that is likely to be impacted by tephra fall, we used Tephra2 (Bonadonna et al. 2005) run within the MATLAB probabilistic wrapper TephraProb (Biass et al. 2016a). Tephra2 provides analytical solutions to the advection–diffusion equation across a grid of evenly spaced points and has been widely utilised to rapidly assess tephra ground accumulation patterns (e.g., Biass et al.2016b; Gjerløw et al. 2022; Warwick et al. 2022). For each eruption scenario that produces tephra fall (five scenarios from *Cont-exp* through *Plin-exp*, see Table 1), we ran 10,000 simulations, each with an eruption source parameter–wind profile combination sampled from distributions (described in the following section and in Online Resource 2).

Model parameterisation

Wind conditions (speed and direction with height) were acquired from the European Centre for Medium-range Weather Forecasts (ECMWF) ERA5 atmospheric reanalysis dataset (Hersbach et al. 2020) for the 10-year period 2014–2023, which is assumed to be sufficient to capture the potential natural variability in wind conditions for the region. The dataset provides hourly profiles at 37 pressure levels on a global 0.25° grid. We considered four profiles per day (0:00, 6:00, 12:00, 18:00) from the record closest to Gede. For each simulation, Tephra2 uses a single wind profile applied directly above the vent. This means the atmosphere is considered vertically stratified but horizontally and temporally homogeneous.

Figure 3 shows the probability of the wind to blow in each direction at various heights in the atmosphere, demonstrating the seasonality in wind conditions across Java.

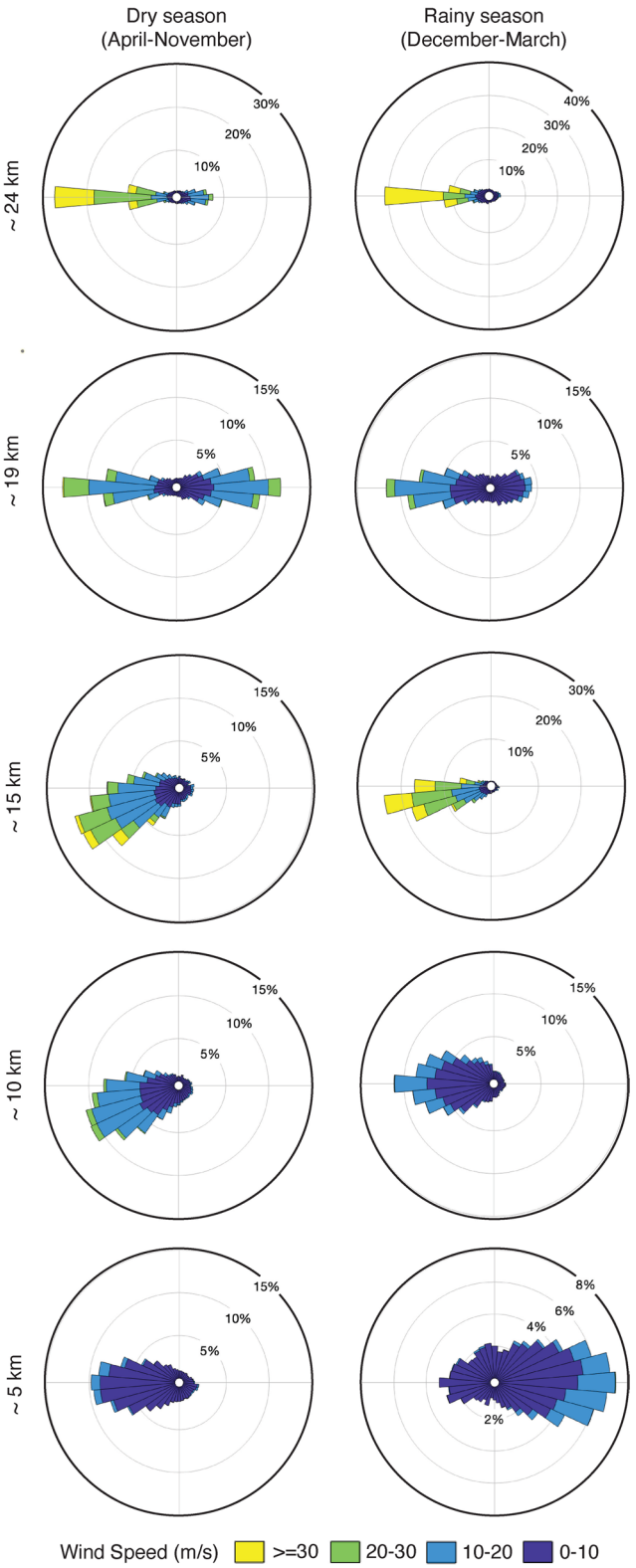

Fig. 3 Wind roses show the probability of wind speed and direction (blowing towards) with height in the atmosphere (km above sea level) at Gede volcano (2958 m asl) during the dry and rainy seasons. Wind data are sourced from ERA5 reanalysis dataset for the time interval 2014–2023 (Hersbach et al. 2020)

During the dry season (April–November), the wind direction is predominantly towards the west or southwest at heights up to ~ 15 km, while in the rainy season (December–March), there is more variation at low levels with winds blowing east at ~ 5 km. During the dry season, there is more variability at greater heights, with an east–west split at ~ 19 km. Given the seasonality in the wind conditions, we ran a set of simulations for both the dry season and the rainy season for each eruptive scenario.

To build distributions for the plume heights associated with each scenario, we used several sources, the min and max values from the GVP bulletins describing eruptions in our Gede plus analogues dataset, values from the modal VEI, and those in Bebbington and Jenkins, (2019). Plume heights were sampled on a logarithmic scale to give preference to the occurrence of smaller values (e.g., Biass and Bonadonna, 2013; Biass et al., 2014; 2017). In the absence of information on total erupted mass or total grain size distribution (TGSD) for Gede or the analogues, we calculated mass from the plume height after Mastin et al., (2009) using a density of 935 kg/m^3 obtained through field work at Gede (Bear-Crozier et al. 2012). For TGSD we expanded the analogue search to look at eruptions globally with characteristics that fit with our eruptive scenarios for Gede, using TGSDs from eruptions at Etna, Italy, (*Cont-exp*), Soufrière St Vincent, St Vincent and the Grenadines (*Int-exp* and *Min-exp*), Chaiten, Chile (*Maj-exp*) and Pinatubo, Philippines (*Plin-exp*).

Cont-exp and *Int-exp* phase eruptions consist of a series of explosions that can last from days to years. In our analogue set, phase durations ranged from 1–850 and 1–1605 days for *Cont-exp* and *Int-exp*, respectively. To model these scenarios, we used the 'Vulcanian' setting within TephraProb (Biass et al. 2016a). For the phase duration, we used a uniform distribution bounded by the 25th –75th percentile durations from the Gede plus analogue dataset. For the repose interval, we used a log-normal distribution between 20 min and 1 h for *Cont-exp* and 1 h and 24 h for *Int-exp*, which gives preference to the lower repose times (Sandri et al. 2014; Biass et al. 2016b).

Large clasts

To identify the area likely to be impacted by large clasts (coarse lapilli: 16–64 mm), we used the particle sedimentation model developed by Rossi et al. (2019) as modified in Jenkins et al. (2022). In the model, particles are released from the clast support envelope at the plume margins, and clast trajectories are calculated by solving the second law of motion in a windy atmosphere. The model has been calibrated and used for probabilistic hazard assessment at Etna volcano, Italy (Osman et al. 2019). As with the tephra fall simulations, we ran 10,000 simulations each for the dry and rainy seasons for the five explosive scenarios; i.e., 10,000 simulations × 2 seasons × 5 scenarios = 100,000 large clast simulations in total.

Model parameterisation

The main model inputs are plume height, which is used to calculate the mass eruption rate after Degruyter and Bonadonna, (2012), the number of particles simulated, particle diameter, density, and three-dimensional wind fields. For the plume height range, we used the same values as for the tephra fall simulations. In each simulation 500 particles were modelled, a value found to be appropriate through sensitivity analysis (Osman et al. 2019). To simplify simulations we used a fixed particle density of 935 kg/m^3 in line with the density of juvenile particles measured in the field at Gede (Bear-Crozier et al. 2012). We used a particle size range attributed to coarse lapilli sized particles with diameters between 16–64 mm (uniform distribution) and the same wind data range as for tephra fall but with the addition of relative humidity and air temperature variables. See Online Resource 3 for the table of input parameters.

Column collapse PDCs

To identify areas at risk of inundation by PDC's resulting from a collapsing column, we used the branching energy cone model: ECMapProb (Aravena et al. 2020). This model is a three-dimensional manifestation of the energy line concept (Heim 1932), which describes the relationship between the drop height (ΔH) and runout length (L) of a flow (ΔH/L). While it does not represent the physical processes operating within a PDC, the energy cone produces results that are comparable with physics-based mass flow models (Tierz et al. 2016). In line with previous studies using the ECMapProb model (Bevilacqua et al. 2021; Aravena et al. 2023), for each of the eruption scenarios, we ran 1,000 simulations, an appropriate number given the simplicity of energy cone type models, which require fewer simulations to achieve stable probability contours compared with more complex models (Online Resource 4).

Model parameterisation

ECMapProb requires the input of two parameters, the collapse height (Ht) and the mobility metric (ΔH/L), along with the topography. For the topography we used the Indonesian National Digital Elevation Model DEMNAS (Geospatial Information Agency 2018) which is a composite of IFSAR, TERRASAR-X, and ALOS data (2010–2015) and has a

resolution of 8.3 m which we resampled to 10 m. Column height ranges used in the tephra fall and large clast simulations were converted to collapse heights under the assumption that column collapse occurs at the top of the gas thrust region (Wilson et al. 1978), which is roughly 10% of the total column height (Sandri et al. 2018; Tierz et al. 2016). The flow mobility metric is dependent on the topography and the dynamics of the flow and should be calibrated and/or tested using field deposits (e.g., Aravena et al. 2020), and supplemented with global datasets as required, so the description of the aleatory variability in flow mobility ideally covers both events that have happened in the past as well as events that could happen in the future (e.g., Tierz et al. 2016). Column collapse type PDC deposits at Gede are limited to a deposit dated at ~ 1 k years BP (Belousov et al. 2015), the deposit has a maximum runout of 7 km towards the southwest, and 4.5 km towards the northeast and was attributed to a VEI 2–3 sized eruption. Using a collapse height of 300–500 m in line with column heights attributed to an eruption of this size, ΔH/L is calculated at 0.22–0.25. We extended this to 0.2–0.3 a range that captures flow mobilities reported in the FlowDat database also for VEI 4–5 eruptions (Ogburn 2012; Tierz et al. 2016), and drew samples from a Uniform distribution within that range. The start location was stochastically sampled from within the Gede crater (Fig. 1c). See Online Resource 4 for the table of input parameters.

Block-and-ash flow PDCs

Gede has experienced dome-forming eruptions in the past (e.g., 1840), and so we considered BAF-type PDCs an important hazard to simulate here; however, there have been no field deposits attributed to this mechanism (Belousov et al. 2015). Given the absence of BAFs in Gede's eruption and deposit record, and the uncertainty in inferring flow generation mechanisms from the GVP bulletin records of analogues, we used the global Flowdat dataset (Ogburn 2012) to parameterise hazard simulations.

To simulate the potential flow paths and inundation areas of BAFs, we used the numerical hazard model Titan2D (Patra et al. 2005). The model simulates granular flows operating over natural terrain, solving the shallow-water equations for the conservation of mass and momentum. Titan2D has been widely used to forecast BAF inundation areas (Sulpizio et al. 2010; Ogburn and Calder 2017; Vázquez et al. 2019). Using Titan2D, we ran 10,000 simulations for the effusive scenario to account for variability in the model inputs. Simulations were carried out as independent, single-core jobs on the Gekko high-performance computing cluster at the Asian School of the Environment, Nanyang Technological University. The mean runtime per simulation was approximately 2 min, and the maximum runtime was ~ 17 h. The complete set of 10,000 simulations took 350 h of CPU time.

Model parameterisation

In our simulations, flows were modelled as a single collapsing pile of material with paraboloid geometry. As with the simulations run for column collapse type PDCs, we used the DEMNAS digital elevation model (DEM). The DEM was reformatted into a GRASS Geographic Information System (GIS) environment for use in Titan2D, which included resampling the resolution from 8.3 m to 10 m. Internal friction angles used in Titan2D have ranged between 15–45° (Stinton et al. 2004; Widiwijayanti et al. 2007; Procter et al. 2009; Sandri et al. 2014; Ogburn and Calder 2017), with several studies showing the relative insensitivity of the model to this parameter within the 15–45° range (Sheridan et al. 2005; Dalbey 2009; Tennant et al. 2021). In all simulations, the internal friction was fixed at 25°. Flows were modelled using the Coulomb rheology.

Titan2D simulations are sensitive to the volume and the basal friction angle. To define an appropriate distribution for BAF volume we looked for a distribution that best fit the 188 BAF volumes within the FlowDat dataset. Using the MATLAB 'fitmethis' function (de Castro 2025) which compares the fit of the 20 built in continuous distributions, we found that the generalised extreme value distribution, where small-volume flows are much more likely than large-volume flows (Online Resource 5), was the best solution. We truncated this distribution to the minimum (0.01 Mm^3) and maximum (210 M m^3) values in FlowDat so that unrealistically high tail end values were not simulated. Since we do not have the field evidence at Gede from which to infer flow mobility we chose a uniform distribution to describe the basal friction angle (Dalbey 2009; Tierz et al. 2018) between 8–30 degrees. These values agree with past studies using Titan2D to simulate flows of this kind (Rupp et al. 2006; Procter et al. 2009; Widiwijayanti et al. 2009; Ogburn and Calder 2017).

For each of the 10,000 simulations, we sampled a volume and calculated the pile height using a pile radius of 150 m informed by the dimensions of the most recent crater (Kawah Ratu). We set a minimum acceptable pile height of 20 m and a maximum of 400 m (informed by the GLADIS database: Harnett et al. 2019). For calculated heights outside of this range, the radius was adjusted to fit the height range. To determine the start location for pile collapse, we used the 1840 lava dome and the locations of more recent eruptive centres to construct a polygon within the Gede crater (radius1 = 450 m, radius2 = 350 m). Coordinates were randomly sampled from within this polygon, assuming an equal probability of flow initiation from any point within. See Online Resource 5 for the table of input parameters.

Lava flows

To identify the area that is likely to be impacted by lava flows, we used the cellular automata lava flow model MOLASSES (Connor et al. 2012). The model does not attempt to capture the rheological properties of lava flows. Instead, lava is "erupted" from a specified location, filling the local topography (grid cell) to a defined thickness before moving downslope into adjacent cells. This process continues until the total erupted volume is distributed across the terrain (Connor et al. 2012). MOLASSES is capable of reproducing flow geometries (e.g., Gallant et al. 2018; Tsang and Lindsay 2020) and has been used for probabilistic lava flow hazard assessments at multiple volcanoes (e.g., Connor et al. 2012; Gallant et al. 2018; Verolino et al. 2022). For the effusive eruption scenario, we ran 10,000 lava flow simulations to account for variability in the model inputs: volume, thickness, and start location.

Model parameterisation

There has been one known lava flow in Gede's eruption history, in 1840 a blocky andesitic flow reached 1.5 km from the lava dome situated within the Gede crater. In our analogue dataset andesitic lava flows are relatively infrequent with only three recorded instances (Karymsky volcano, 1970; 2002; Lewotobi volcano, 2024). MOLASSES inputs are distributions for the total flow volume, and residual thickness which is the minimum thickness that must be retained in a grid cell before lava is passed onto the next grid cell, pulse volume–the volume released at one time (Connor et al. 2012) and the start location. Given the limited amount of information that can be obtained from Gede or the analogue dataset, we looked for literature describing andesitic lava flows globally and consequently parameterised our lava flow simulations using flow volumes and thicknesses from eruptions at El Reventador, Ecuador (Arnold et al. 2019), Colima, Mexico (Carrara et al. 2019), and Karangetang, Indonesia (Global Volcanism Program 1976). For the residual thickness we set a uniform distribution between 8.3–30 m, informed by the minimum thickness described in the global analogues and the flow front thickness of the 1840 flow at Gede (mapped by Belousov et al. 2015). For the total erupted volume, we measured the surface area of the erupted material at Gede and used a homogenous thickness of 30 m, to obtain a volume of 24.9 x $10^6 m^3$. This is large when compared to volumes in the analogue set, therefore we used this as the upper bound of the distribution, and the lowest value from the analogue set as the lower bound. We set a uniform distribution for the volume to reflect maximum uncertainty. For the pulse volume we used a uniform distribution between 1 x $10^4 m^3$- 1 $\times 10^5 m^3$ based on Connor et al. (2012) who suggest this as a typical range. For the starting location, we used the same polygon and sampling strategy as for BAF simulations. See Online Resource 6 for the table of input parameters.

Preparation of hazard outputs and hazard intensity thresholds

In this work hazard models were used to produce either binary hazard inundation footprints (column collapse, lava flows, block-and-ash flows) or a quantitative measure of impact severity; mass accumulation (kg/m^2) for tephra fall, impact energy (Joules) for large clasts. For binary outputs, we contoured probabilistic outputs as probabilities of 1, 5, 10, 25, 50, 75, 95%, where the area enclosed within the 1% contour has at least 1% probability of being inundated and the area enclosed with the 95% contour has at least 95% probability of being inundated.

For tephra fall and large clasts, we produced hazard curves for the locations relevant to each hazard out of the nine locations marked in Fig. 1a. Hazard curves show the probability (y-axis) of exceeding a given hazard intensity (x-axis). Even though hazard impacts are expected to scale with the hazard intensity, particularly of dynamic pressure (e.g., Valentine, 1998; Zuccaro et al. 2008; Jenkins et al. 2013), the former are too complex to be properly captured with the most widely used PDC models, like TITAN2D. Hence, we did not produce hazard curves for flow hazards because the relationship between hazard intensity metric and impact is not clear; for example, a PDC may leave minimal deposit and exert very low dynamic pressures at a given location, yet still cause fatalities (Jenkins et al. 2013; Baxter et al. 2017; Dellino et al. 2021).

Locations for hazard curve calculations for tephra fall and large clasts were chosen for their high population densities, cultural significance (the Cipanas presidential palace located in Cibodas), or as locations where people are expected to gather (national park office, hot springs waterfall within the national park). For tephra fall from prolonged phases (the *Cont-exp* and *Int-exp* scenarios); in addition to the final accumulation after the full duration of the eruption, we produced hazard curves showing the exceedance probabilities of the minimum and maximum mass accumulation from each explosion within the eruption, and curves showing the cumulative accumulation over time from consecutive pulses. Curves for the minimum and maximum mass accumulation represent the lower and upper bounds of accumulation expected on the ground from individual explosions within a multi-explosion eruption, while the cumulative accumulation can be used to understand the rate of accumulation for these prolonged eruptions.

For tephra fall and large clasts we also prepared percentile hazard outputs showing the hazard intensity (tephra accumulation or impact energy) at the 5th, 50th, and

95th percentiles. The 5th percentile hazard output indicates a low hazard intensity situation, i.e., 95% of hazard intensities are greater than this; the 50th is the median hazard intensity, and the 95th percentile corresponds to a high hazard intensity, i.e., only 5% of simulations have hazard intensities greater than this. To contextualise our findings, we contoured the hazard intensities at impact thresholds that are relevant for the exposed elements around Gede (Table 2). Thresholds should be used as a guideline to infer the potential impacts, which can occur above or below the thresholds cited. In particular, the susceptibility of exposed elements to different hazard intensities is challenging to quantify due to differences within the same asset class; for example, with buildings, factors such as the quality of construction material and the age of the building can affect the ability to withstand tephra fall loading (Jenkins et al. 2015).

Results

Tephra fall

Tephra fall hazard for the three smaller eruptive scenarios (*Cont-exp*, *Int-exp* and *Min-exp)* is largely influenced by seasonal wind patterns. For these scenarios, there is a clear difference between the rainy and dry seasons; the main dispersion direction is west in the dry season and east in the rainy season (Fig. 4). For the larger eruption scenarios *(Maj-exp, Plin-exp)*, this seasonal variation is less pronounced (Fig. 5).

Due to the prevailing wind directions around Gede, a large eruption (*Maj-exp, Plin-exp* scenario) is needed for significant tephra accumulation at Jakarta and its international airport (Soekarno-Hatta) (Fig. 5). There is an 80% probability of 0.1 kg/m^2 (sufficient to disrupt airport operations) from a *Plin-exp* scenario and 50% probability of the same accumulation from a *Maj-exp* scenario (Fig. 6).

Bandung city (~ 70 km east of Gede) is more likely to be affected by the prolonged eruption scenarios (*Cont-exp*, *Int-exp*) than Jakarta; however, the probability of exceeding 1 kg/m^2 is still less than 0.1% (Fig. 6). For the discrete eruption scenarios which deposit material over the course of hours rather than days, a *Maj-exp or Plin-exp* eruption has at least a 2% probability of tephra accumulation sufficient to obscure road markings and incur significant clean-up (1 kg/m^2) (Fig. 6).

The city of Bogor (~ 30 km northwest of Gede) is likely to be affected by tephra fall from all eruption scenarios excluding the *Int-exp* scenario. A *Cont-exp* eruption has a 1% probability of accumulation that is sufficient to obscure road markings after successions of explosions over the course of 7 days (Fig. 6). From a *Min-exp* scenario there is a 10% probability of accumulations exceeding 0.1 kg/m^2 and from a *Maj-exp* scenario there is a 10% probability of tephra accumulation that is sufficient to require cleaning of power lines (5 kg/m^2). A *Plin-exp* scenario has the potential to cause building damage in Bogor; with a 35% probability of exceeding 50 kg/m^2 during the rainy season and 20% during the dry season (Fig. 6).

For the locations that lie in the almost continuous high population density ring that surrounds Gede (Cigombong, Cianjur, Sukabumi, Cibodas) tephra accumulations that are sufficient to cause building damage can be expected from a *Maj-exp* or *Plin-exp* eruption scenario (Fig. 6). Such accumulations are not expected at these locations

Table 2 Hazard intensity thresholds considered for tephra fall and large clast hazards

Hazard intensity	Expected impact
Tephra mass accumulation	
0.1 kg/m^2	• Disruption of airport operations (Blake et al. 2017)
1 kg/m^2	• Road markings obscured (Jenkins et al. 2015) • Disruption of harvest operations for arable crops and rice paddies (Jenkins et al. 2015)
5 kg/m^2	• Minor crop productivity loss for trees and ground crops • Power lines require cleaning (Jenkins et al. 2015)
50 kg/m^2	• Moderate damage to Indonesian style buildings (Williams et al. 2020)
100 kg/m^2	• Heavy damage to Indonesian style buildings (Williams et al. 2020)
500 kg/m^2	• Power lines and airports beyond economic repair (Jenkins et al. 2015)
Large clast impact energy	
0.15 Joules	• Penetration of glass skylights or windows that are 2.5–4 mm thick occurs at 0.15–2 Joules (Jenkins et al., 2014)
10 Joules	• Penetration of clay or terracotta roof tiles that are 10–40 mm thick occurs at 10–80 Joules (Jenkins et al., 2014, after Blong 1981, Pomonis et al., 1999). Roof tiles for buildings around Kelud volcano are 15 mm thick (Williams et al. 2020)
28 Joules	• Human skull fracture (Yoganandan et al. 1995)

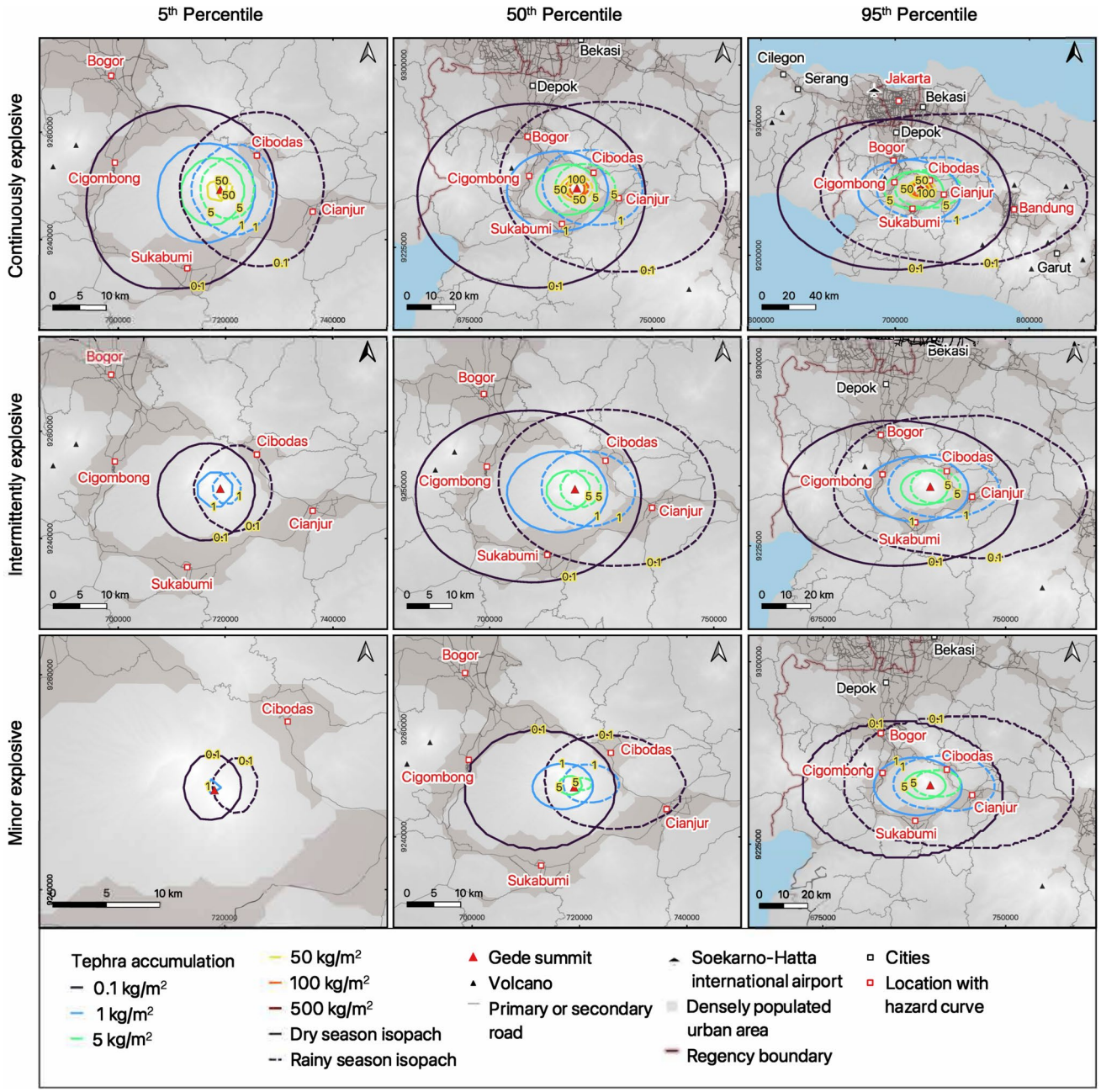

Fig. 4 Hazard outputs showing tephra fall mass accumulation for the continuously explosive (Cont-exp), intermittently explosive (Int-exp), and minor explosive (Min-exp) eruption phases. Mass accumulations are presented as fixed percentiles of 5th, 50th, and 95th for each scenario. Contour values were chosen to reflect important impact thresholds (Table 2). Tephra was modelled using TephraProb (Biass et al. 2016a). Densely populated urban areas from: Pesaresi and Panagiotis 2023. Base map: ESRI shaded relief and SRTM (2000). Coordinate reference system: EPSG: 32748

from the smaller eruption scenarios (< 0.1% exceedance probability), however Fig. 4 shows that the final tephra accumulation for a continuously explosive eruption is sufficient to cause productivity loss to crops (5 kg/m^2) in this heavily cultivated area.

Large clasts

Similarly to the tephra fall hazard, we found that the dispersion of large clasts for the *Cont-exp, Int-exp*, and *Min-exp* scenarios is more influenced by the seasonal wind directions

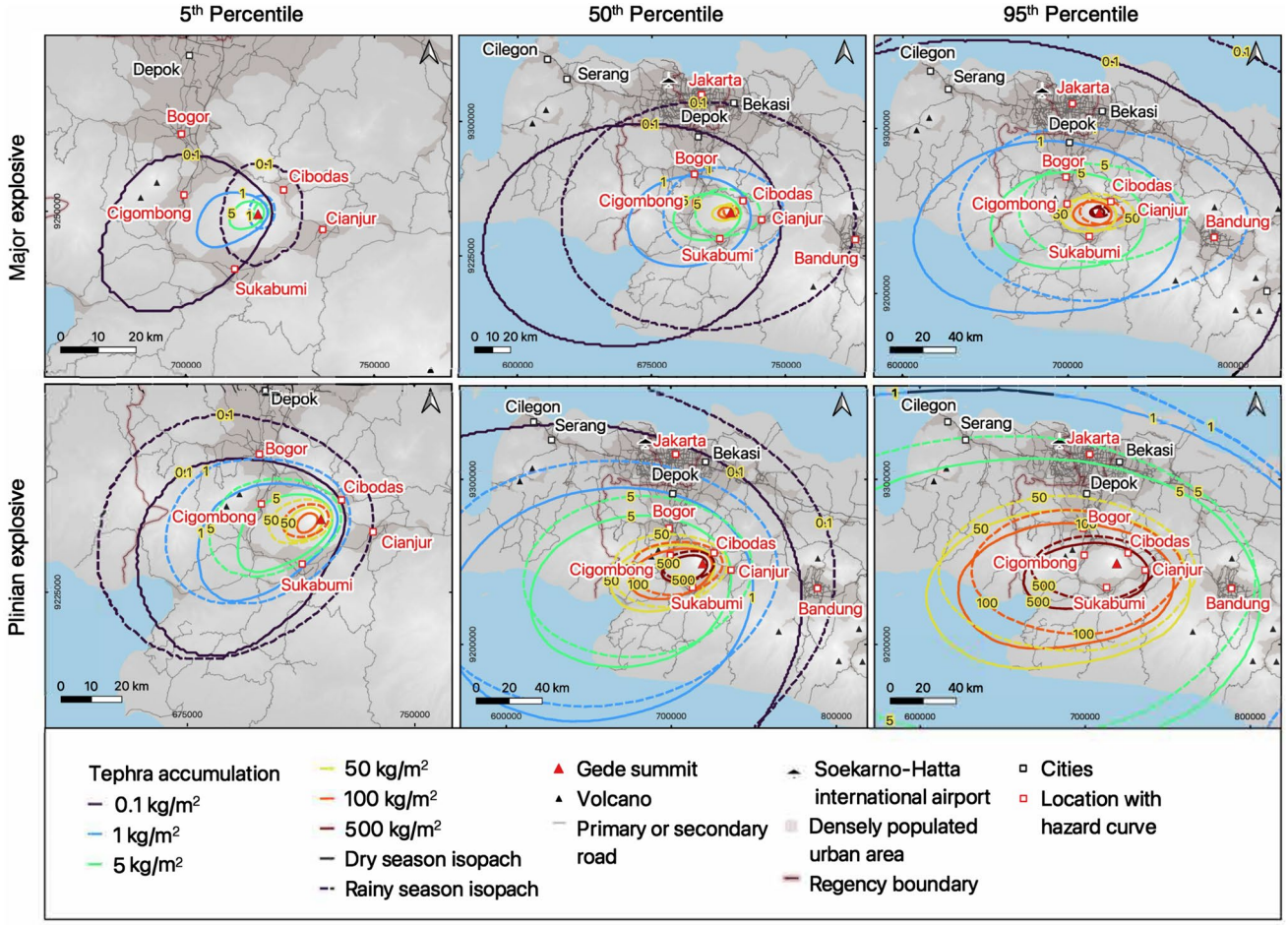

Fig. 5 Hazard outputs showing tephra fall mass accumulation for the major explosive (Maj-exp) and Plinian (Plin-exp) explosive eruption phases. Mass accumulations are presented at fixed percentiles of 5th, 50th, and 95th for each scenario. Contour values were chosen to reflect important impact thresholds (Table 2). Tephra was modelled using TephraProb (Biass et al. 2016a). Densely populated urban areas from: Pesaresi and Panagiotis 2023. *Base map: ESRI shaded relief and SRTM (2000). Coordinate reference system: EPSG: 32748*

than for the larger eruption scenarios (Figs. 7, 8, 9). For the *Cont-exp, Int-exp*, and *Min-exp* scenarios, clasts are deposited towards the east during the rainy season and towards the west during the dry season (Fig. 7). For the *Maj-exp* and *Plin-exp* scenarios, the effect of the seasons is less, and the dispersion axis is oriented slightly towards the southwest direction throughout the year (Fig. 8). The Gede-Pangrango national park is elongated in the southwest direction and extends up to ~ 17 km away from the summit of Gede. The national park status limits development and means that the densely populated areas are farther away from the volcano in the southwest direction.

For the *Cont-exp, Int-exp*, and *Min-exp* eruption scenarios, there is a low probability that large clasts with sufficient energy to cause harm will be dispersed farther than a few km away from the summit. The 95th percentile hazard output shows that clasts with an impact energy of > 28 J (sufficient to cause human skull fracture) can reach up to ~ 2 km away for the *Cont-exp* scenario, ~ 2.5 km for the *Int-exp* scenario, and up to ~ 3 km for the *Min-exp* scenario.

Larger eruption scenarios, the *Maj-exp* (column height 10–20 km) and *Plin-exp* (column height 20–30 km), can result in impact energies that are capable of damaging buildings in the area surrounding the national park. For a *Maj-exp* scenario, there is a ~ 10% probability of sufficient impact energy to damage glazed openings (> 0.15 J) at Cipanas presidential palace, ~ 1% at Cianjur, and 3% at Sukabumi (Fig. 9). The probability of sufficient energy for roof tile penetration (10 J) in these locations is 5%, < 0.1%, and 0.5%, respectively. For a *Pl-exp* scenario, there is a 90% probability of sufficient impact energy to damage glazed openings at Cipanas presidential palace, 80% at Sukabumi, 10% at Bogor, and 50% at Cigombong.

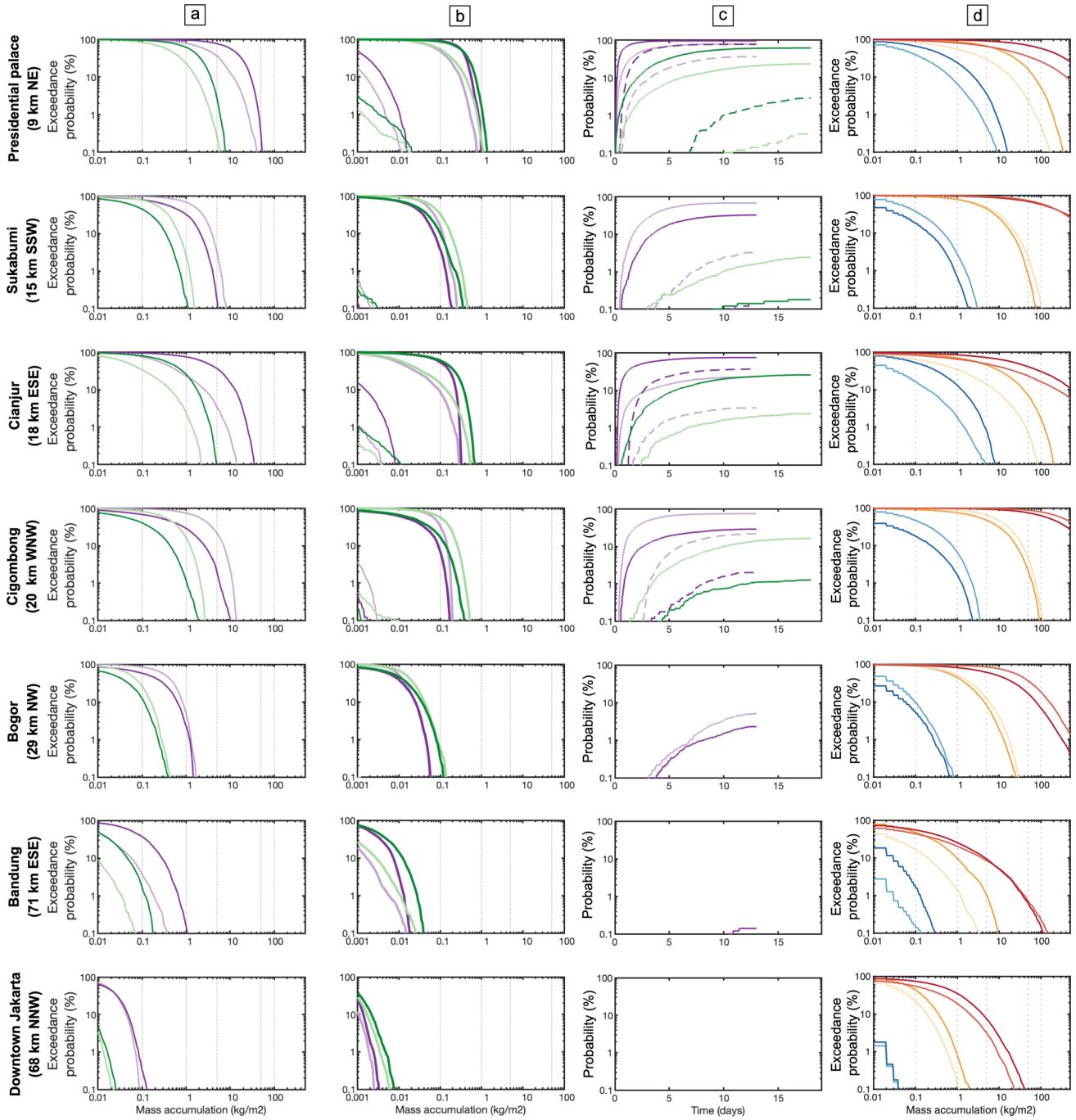
a
b
c
d
Presidential palace (9 km NE)
Sukabumi (15 km SSW)
Cianjur (18 km ESE)
Cigombong (20 km WNW)
Bogor (29 km NW)
Bandung (71 km ESE)
Downtown Jakarta (68 km NNW)
Exceedance probability (%)
Probability (%)
Mass accumulation (kg/m2)
Time (days)
Cont-exp dry
Cont-exp rainy
Int-exp dry
Int-exp rainy
min max Cont-exp dry
min max Cont-exp rainy
min max Int-exp dry
min max Int-exp rainy
1 kg/ m² Cont-exp dry
5 kg/ m² Cont-exp dry
1 kg/ m² Cont-exp rainy
5 kg/ m² Cont-exp rainy
1 kg/ m² Int-exp dry
5 kg/ m² Int-exp dry
1 kg/ m² Int-exp rainy
5 kg/ m² Int-exp rainy
Min-exp dry
Min-exp rainy
Maj-exp dry
Maj-exp rainy
Plin-exp dry
Plin-exp rainy

◂**Fig. 6** Curves showing the hazard at specific locations around the volcano marked on Fig. 1. The first three columns plot data from the prolonged eruption scenarios (duration > 1 day) (Continuously explosive, Intermittently explosive), and the final column plots the discrete scenarios (duration < 1 day) (Minor explosive, Major explosive, Plinian explosive). **a** Exceedance probabilities of the final tephra accumulation at the end of multi-explosion eruption for the prolonged scenarios; **b** Exceedance probabilities of tephra accumulation associated with the smallest and largest explosions from each of the 10,000 simulated eruptions for both of the prolonged scenarios. These represent the lower and upper bounds of accumulation expected on the ground from individual explosions within a multi-explosion eruption. **c** The probability that the accumulation from repeated explosions occurring throughout the course of the eruption for the prolonged scenarios will exceed 1 kg/m^2 and 5 kg/m^2 over time. **d** Exceedance probabilities of tephra accumulation from the discrete eruption phases. Grey vertical lines mark impact thresholds that are relevant for the exposed elements around Gede (Table 2)

In addition to the potential damage to physical assets, for a *Maj-exp* eruption scenario there is at least a 3% probability that clasts will have sufficient energy to cause skull fracture (> 28 J) at Cibodas, and ~ 0.2% at Sukabumi. For a *Plin-exp* scenario, the probability of this is 30% at the presidential palace, 15% at Cianjur, 20% at Sukabumi, and 10% at Cigombong (Fig. 9).

Column collapse PDCs

A collapsing column from any of the discrete eruption scenarios simulated (*Min-exp, Maj-exp, Plin-exp*) is likely to impact Cibodas, the closest town to the volcano at ~ 7 km distance. For the *Min-exp scenario*, there is at least a 75% probability of inundation at Cibodas (Fig. 10). Gede's crater is breached towards the north (Fig. 1c); for the *Min-exp scenario* that features lower column collapse heights than the *Maj-exp* and *Plin-exp* scenarios, this northwards breach and the lower crater wall height towards the southwest affects the directionality of flows and results in higher inundation probabilities in the northeast and southwest flanks of the volcano (Fig. 10). The maximum extent (within the 1% probability contour) of PDCs resulting from the *Min-exp* scenario is ~ 15 km in the northeast direction. In addition to the high probability of inundation at Cibodas, there is ~ 20% probability that Cianjur and Sukabumi will be affected by a *Min-exp* scenario. For the *Maj-exp and Plin-exp* scenarios, which have maximum column heights of up to 20 km and 30 km respectively, the inundation distribution is more radial around the volcano; the maximum extent for a *Maj-exp* scenario is ~ 20 km, while for the *Plin-exp* scenario this is ~ 26 km. For both scenarios, there is at least a 95% probability that Cibodas will be inundated; for the maximum scenario, this probability contour also includes the edges of Sukabumi and Cianjur that are more proximal to the volcano (Fig. 10). For the *Plin-exp* scenario, approximately half of Sukabumi and Cianjur are included within the 95% probability contour.

Block- and-ash flow PDCs

Probabilistic simulations indicate that future block-and-ash flows at Gede are likely to inundate the northeast sector of the volcano, although there is a 1–5% probability of inundation of the upper southwest flank (Fig. 11). Block-and-ash flow travel direction is largely controlled by the summit topography. The northwards breach in the crater and the presence of a remnant of the previous crater wall, known as the Sela rock (Fig. 1c), direct the majority of flows towards the northwest at the summit. Flows are largely channel confined with higher inundation probabilities in the Ci Kundul and Ci Pendawa drainages (Fig. 11a). The dominant northeast and southwest travel directions of block-and-ash flows agree with the work of Tennant et al. (2023), who coupled a topography-based methodology for forecasting flow directionality with a recalibrated version of the LaharZ model to gain insight into flow directions at Gede. Our simulations show that the maximum expected runout (1% probability) is ~ 9 km in the Ci Kundul channel and ~ 11 km in the Ci Pendawa channel (Fig. 11). The majority of simulated flows (90%) had runouts less than 4 km; however, there is a 1–5% probability that the densely populated town of Cibodas will be inundated. As shown in Fig. 11, there is a branching of flows at the summit. Most simulated flows travel around the Sela rock towards the northwest, entering the Ci Kundul channel and are subsequently diverted towards the NE by Pangrango volcano and the northeasterly oriented ridge.

Lava flows

Simulations of blocky andesitic style lava flows at Gede show that flows are expected to remain within ~ 3 km of the summit area. Flows follow the summit topography with the breached crater directing them towards the Ci Kundul and Ci Pendawa drainages located in the north to northeast sector of the volcano (Fig. 11). The two northern branches of the simulated footprint are separated from the northeast branch by a remnant of the crater wall and topographic high, Sela ridge. There is a 50% probability that flows will remain within 1 km of the summit area.

Discussion

In this work, we have produced hazard outputs for five different hazards from six different scenarios that are possible at Gede. The analysis presented in this work is relevant for the next eruption at Gede. For future eruptions beyond this,

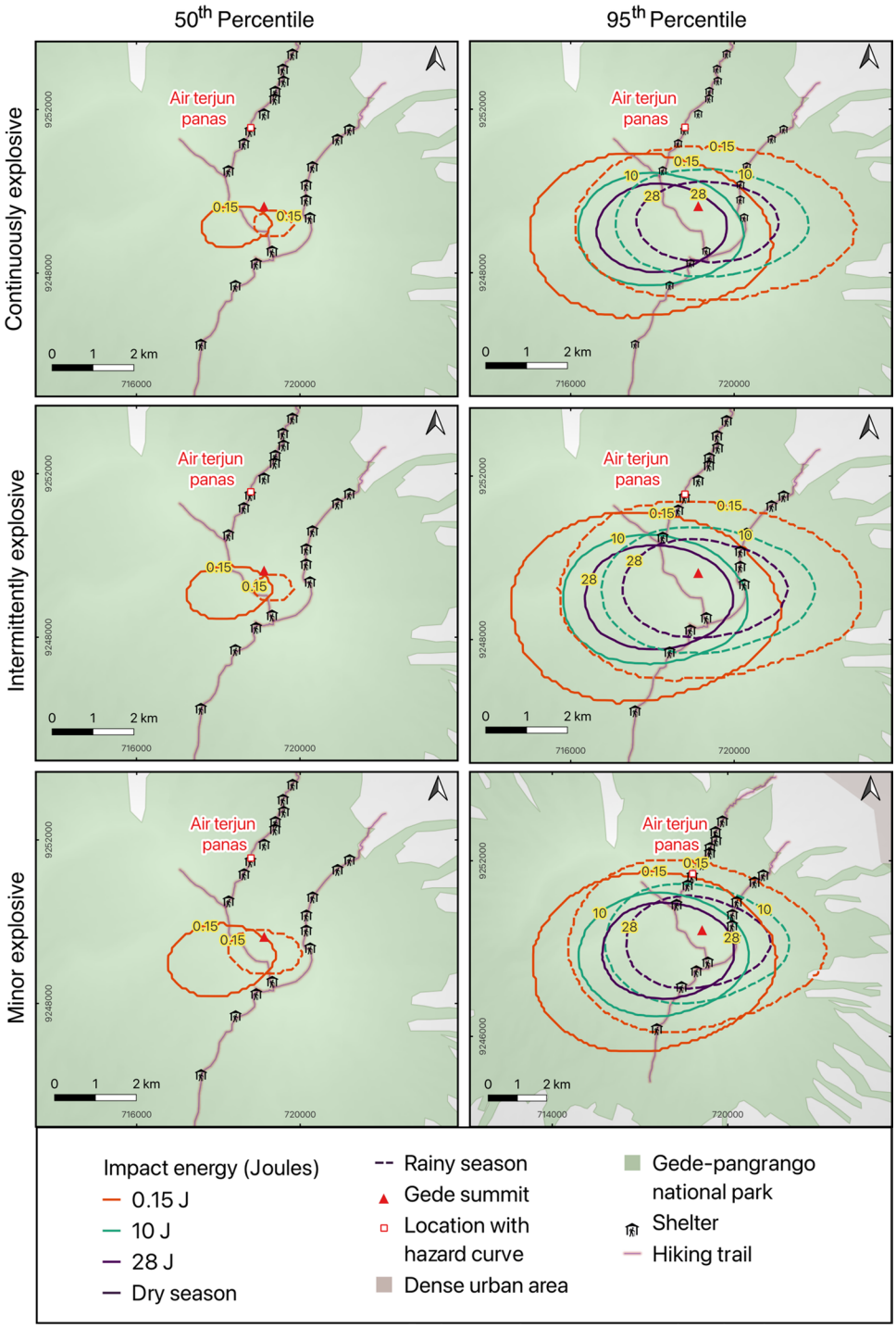

Fig. 7 Hazard outputs showing the impact energy associated with the sedimentation of large clasts (16–64 mm in diameter) for the continuously explosive (Cont-exp), intermittently explosive (Int-exp), and minor explosive (Min-exp) eruption scenarios. Impact energies are presented at the 50th and 95th percentile for each scenario. The 5th percentile hazard produced impact energies that were below the minimum hazard intensity threshold and are not shown. Contour values were chosen to reflect important impact thresholds (Table 2). Large clast deposition was modelled using the model of (Rossi et al. 2019). Base map: ESRI shaded relief and SRTM (2000). Coordinate reference system: EPSG: 32748

any topographic changes from the deposition or erosion of new material would require a reassessment to confirm that this analysis remains valid.

The produced outputs are contingent on the vent remaining within the (~ 700 × 900 m diameter) Gede crater. To account for potential variations in the vent position within the Gede crater, we incorporated uncertainty in the starting locations of lava flows, column collapse PDCs, and BAFs. For tephra fall and large-clast simulations, the DEM resolution made this unnecessary. All recorded Holocene activity at Gede has occurred from within the Gede crater; the 1840 lava dome is punctuated by several younger explosive centres: Ratu (most recent), Baru, and Lanang craters, which are located a couple of hundred meters apart (Belousov et al. 2015). We did not consider the potential for vent migration outside of the Gede crater or the occurrence of flank

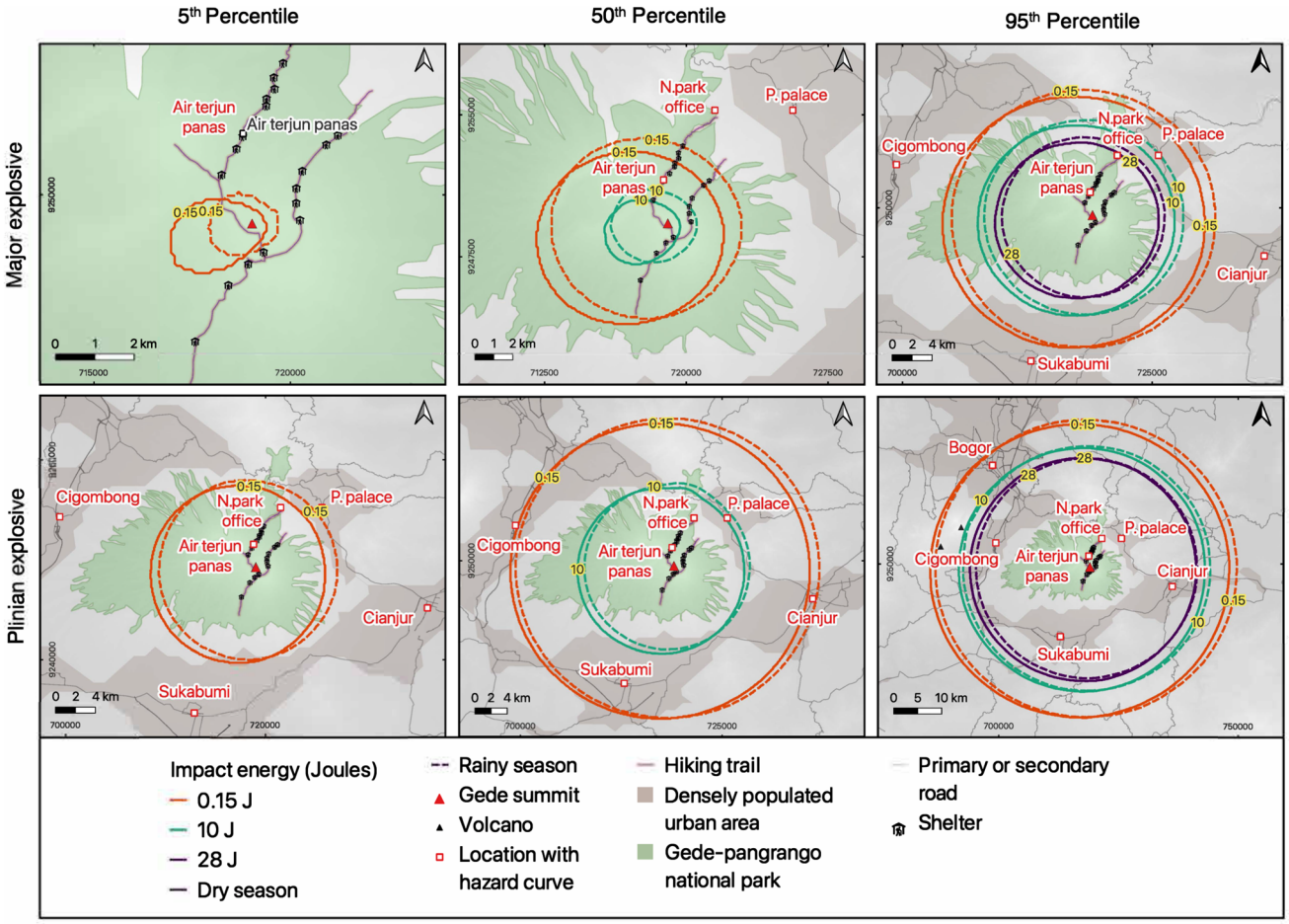

Fig. 8 Hazard outputs showing the impact energy associated with the sedimentation of large clasts (16–64 mm in diameter) for the major explosive (Maj-exp) and Plinian explosive (Plin-exp) eruption scenarios. Impact energies are presented at the 5th, 50th, 95th percentile for each scenario. Contour values were chosen to reflect important impact thresholds (Table 2). Large clast deposition was modelled using the model of Rossi et al. (2019). Densely populated urban areas from: Pesaresi and Panagiotis (2023). Base map: ESRI shaded relief and SRTM (2000). Coordinate reference system: EPSG: 32748

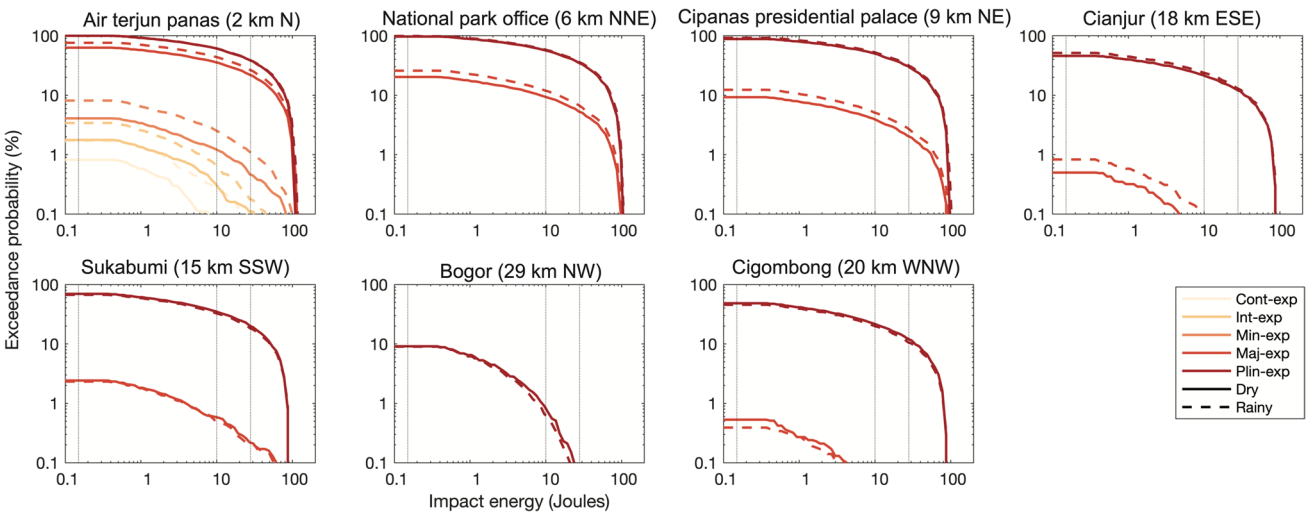

Fig. 9 Hazard curves show the exceedance probabilities of large clast impact energy for the different eruptive phases at locations around the volcano marked on Fig. 2. Grey vertical lines mark impact thresholds that are relevant for the exposed elements around Gede (Table 2)

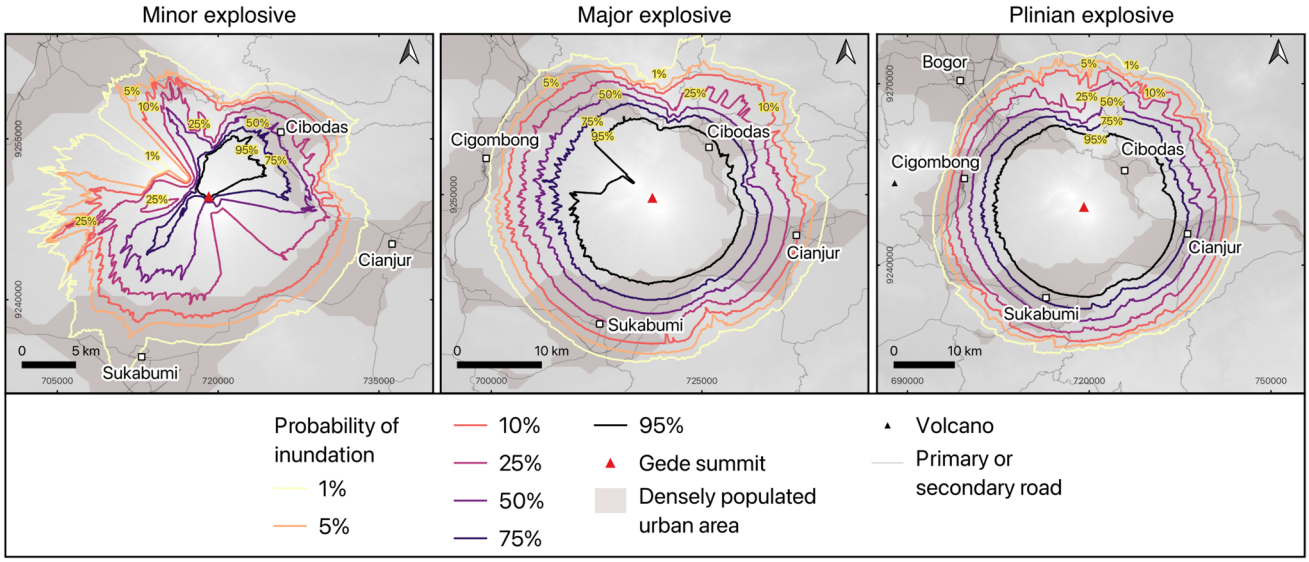

Fig. 10 Hazard outputs showing the probability of inundation by column collapse type pyroclastic density currents for: **a**) the Minor explosive (Min-exp) eruption scenario, **b**) the Major explosive (Maj-exp) eruption scenario, and **c**) the Plinian (Plin-exp) eruption scenario. Inundation was modelled using ECMapProb (Aravena et al. 2020). Densely populated urban areas from: Pesaresi and Panagiotis (2023). Base map: ESRI shaded relief and SRTM (2000). Coordinate reference system: EPSG: 32748

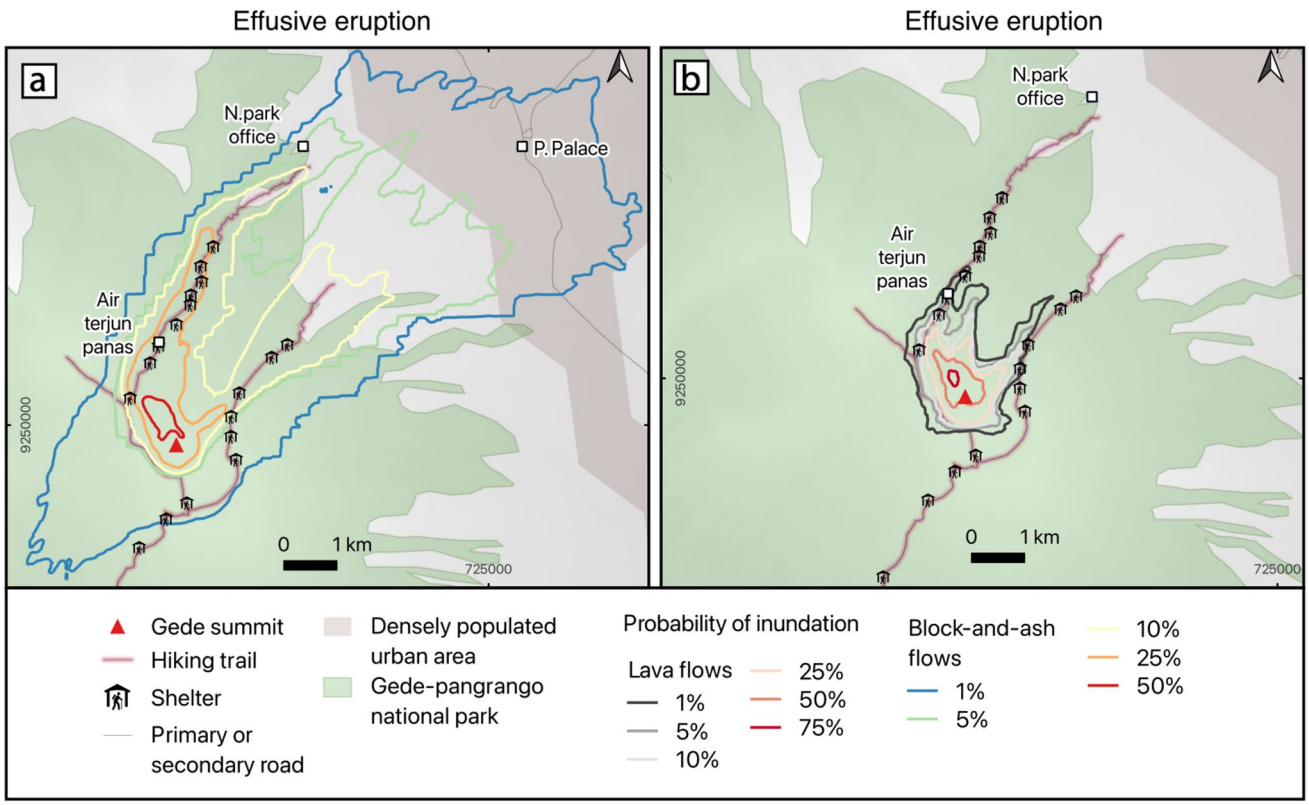

Fig. 11 Hazard outputs showing the probability of inundation by hazards associated with an effusive eruptive scenario; **a**) inundation by block-and-ash flows modelled using Titan 2D (Patra et al. 2005), and **b**) inundation by andesitic lava flows modelled using MOLASSES (Connor et al. 2012). Densely populated urban areas from: Pesaresi and Panagiotis (2023). Base map: ESRI shaded relief and SRTM (2000). Coordinate reference system: EPSG: 32748

eruptions. Should monitoring data during renewed unrest indicate an elevated likelihood of a flank eruption, this hazard assessment would require re-evaluation.

In our characterization of tephra fall hazard, simulations do not account for surface remobilisation of deposits, which can lead to secondary deposition in areas with strong winds, sparse vegetation, and low soil moisture (Folch et al. 2014). In the wind data interval analysed (2014–2023), surface winds to ~ 500 m asl at Gede show a dominant north-northeast direction year-round (Hersbach et al. 2020). This raises the possibility that remobilised deposits could be transported towards Jakarta. In the past, tephra fall has in fact been reported in Jakarta during the 1948 Gede eruption (Petroeschevsky 1952). This eruption is categorised in the phases dataset as a seven-phase eruption consisting of five minor explosive phases and two intermittently explosive phases (Bebbington and Jenkins 2022). Tennant et al. (2021) found that it was not possible to reconstruct the eruption using Tephra2 given the wind conditions at the time of the eruption and the reported column heights. This led to the suggestion that either the report was incorrect, the resolution of the meteorological data was insufficient, or that Tephra 2 was unable to resolve the apparently small accumulation. Remobilisation of material from earlier phases in the eruptive sequence is an alternative explanation for this discrepancy and suggests that the city may not be entirely free from tephra fall following small eruptions. This work might be extended to consider the potential for surface remobilisation of deposits. In addition to modelling the ground accumulation with Tephra2, 3D dispersion models such as Fall3D (Folch et al. 2020) might also be applied to assess airborne ash concentrations, which are critical for determining safe flight zones.

Large clasts from the *Cont-exp*, *Int-exp*, and *Min-exp* eruption scenarios did not travel further than ~3 km from the source. While these distances are within the Gede-Pangrango national park limits and clasts do not travel sufficiently far to reach populated areas, they do pose a threat to human life for anyone on the hiking trails within the national park (in addition to the hazard posed by ballistic projectiles). Shelters with concrete roofs that are positioned along the trails may be able to withstand impact energies associated with not only large clasts but also ballistic projectiles. The ability to withstand penetration depends on the level of reinforcement; fibre clad (reinforced) concrete slab 4.5–9.5 mm thick is penetrated at impact energies between 20–85 J, which is within the range produced by large clasts, while for roofs with steel reinforced concrete slabs, larger impact energies are required for penetration (4,000–12,000 J) (Blong 1981). However, backside peeling/scabbing can occur at lower impact energies than those typically required for penetration (Williams et al., 2017). Peeled concrete fragments ejected from the underside of the slab can have velocities of up to 37% of the ballistic projectile (Williams et al., 2017), which may cause harm to anyone sheltering inside.

Limitations

- As with any simulation-based hazard assessment, uncertainty arises from the use of models to represent the complex physical processes of volcanic hazards. In this study, we used straightforward models to forecast the spatial extent of hazardous phenomena. These were selected as a trade-off between the ability to reproduce realistic hazard footprints and the need to run large numbers of simulations to capture input and output uncertainty. More advanced models that better reproduce the physical processes would require characterization of more extensive inputs and require more processing power limiting the number of simulations that could be explored to capture uncertainty.
- Large clast simulations were the most computationally demanding out of the five hazards simulated. To facilitate the modelling, we did not account for different particle densities (juveniles and lithics) instead we used the density associated with the juvenile clasts. This is likely to have resulted in larger hazard footprints, and lower impact energies than if higher density lithic fragments were also simulated.
- Due to limited geological and historical data for Gede, hazard model input parameters were partly derived from analogue volcanoes and global datasets. While analogue selection methods were applied systematically, this approach inevitably influenced the results. Further research is needed to assess how analogue choice affects hazard assessment outcomes.
- The use of global datasets introduces potential biases such as over-representation of specific eruptions that are well characterised. The use of the Global Volcanism Program data to help define plume heights for some scenarios also carries uncertainty due to the default VEI 2 assignment, which may not reflect their true intensity.
- For lava flow, column collapse PDC and block-and-ash flow simulations, starting locations were sampled uniformly from within the Gede crater, assuming equal likelihood for all points. This could be refined by incorporating the positions of past eruptive centres within the crater to better reflect initiation sites.

Future perspectives

Future studies may allow for the extension of this work through consideration of additional hazards currently not included, such as debris avalanches, syn- and post-eruptive lahars, ballistic projectiles, volcanic gases, and fires caused

by volcanic activity, along with alternative PDC generation mechanisms (e.g., boiling over, lateral blasts). In addition to the hazards associated with magmatic eruptions, phreatic eruptions have been known to occur at Gede; these are particularly dangerous as they can occur with little precursory activity (Barberi et al. 1992; Stix and de Moor 2018). In the absence of additional field data, the continued development of open access global datasets (e.g., Mastin et al. 2009; Ogburn 2012; Bebbington and Jenkins 2022) is vital for supporting volcanic hazard assessment (Tierz 2020).

West Java is very seismically active (Supendi et al. 2018); the Cimandiri fault is ~ 8 km south of Gede, and the Cianjur fault is ~ 7 km towards the east (Supendi et al. 2018). Future seismic activity close to Gede could result in the collapse of the unstable remaining section of the northeast crater wall Sela rock (Belousov et al. 2015) and the generation of a debris avalanche. Due to the location of Sela rock (Fig. 1c), this is likely to be directed towards the northeast, though more work needs to be done to understand the specific conditions that could lead to its collapse along with the expected inundation area.

This work provides a step towards the assessment of volcanic risk from Gede volcano. To move this work further requires quantification of the relevant exposure and vulnerability to the simulated hazards. This includes gathering geospatial information for population, buildings, road, rail, and power networks and any other relevant assets. The impact thresholds that are highlighted in this work for tephra fall and large clasts are based on the available published literature for assets that are closest to those present in our area. However, these are often based on limited empirical evidence. The collection of empirical damage data either through ground surveys (e.g., Blong 2003; Jenkins et al. 2015; 2024a, b) or by developing methods for remote data collection (e.g., Williams et al. 2020; Lerner et al. 2022; Tennant et al. 2024) is a priority for developing robust vulnerability estimates. The work might also benefit from the consideration of interactions between cascading hazards, which are currently treated separately but can affect the vulnerability of exposed assets (e.g., Zuccaro and De Gregorio, 2013; Williams et al. 2019).

Conclusions

Gede is an active volcano with ~ 440,000 people living within 10 km of the summit, and a further ~ 70,000 annual visitors. As a step towards assessing the risk posed by this volcano, we have conducted the first fully probabilistic hazard assessment for Gede. Our assessment consisted of > 200,000 unique simulations for five hazardous phenomena from six eruptive scenarios. With 23 confirmed eruptions at Gede constrained to the last 277 years, and limited geological or historical evidence of these eruptions, this work relied on analogue volcanoes and global datasets to supplement eruption information and enable a comprehensive forecast of potential future scenarios.

Our findings highlight that tephra fall and large clast sedimentation are strongly controlled by seasonal variation in wind directions, with a predominant wind direction towards the east during the rainy season and west during the dry season at plume heights associated with continuously, intermittently, and minor explosive eruption scenarios. Under these wind patterns, Jakarta (~ 60 km from Gede's summit) is unlikely to be affected by tephra fall from eruptions of this size, although remobilisation of deposits could be a potential source of tephra in the capital. Furthermore, larger sized eruptions with plume heights greater than 10 km are expected to impact the city. Closer to the volcano in the densely populated ring that surrounds the national park, building damage is possible from both tephra fall and large clasts from a major or Plinian eruption. All eruption scenarios are expected to produce sufficient tephra fall accumulation in these areas to disrupt road markings and incur significant clean-up.

We found that block-and-ash flow type PDCs are expected to follow the topography. The breached crater at Gede results in dominant travel directions towards the northeast, with flow runouts in this direction that are sufficient to reach Cibodas town, 7 km to the northeast. PDCs from a collapsing column from the minor explosive eruption scenario (column height 1–10 km) can extend up to ~ 15 km from the summit, but could reach up to ~ 20–25 km for major and Plinian eruptions that have column heights of 10–20 km and 20–30 km, respectively. Blocky andesitic style lava flows are expected to travel towards the northeast; however, they are likely to remain within ~ 3 km of the summit area.

Our work lays a critical foundation for future risk assessment at Gede, emphasizing the need for more detailed local field data that may be used to refine hazard models and their assumptions. Such efforts will be crucial in improving the accuracy of hazard forecasts and ultimately enhancing the resilience of communities surrounding the volcano.

Supplementary Information The online version contains supplementary material available at https://doi.org/10.1007/s00445-025-01908-y.

Acknowledgements We are indebted to Eduardo Rossi for sharing the large clast sedimentation model, and to Sébastien Biass for the modifications. We are very grateful to Hetty Triastuti and Hendra Gunawan for sharing their invaluable expertise and recognize the contributions of Fidel Costa and Chris Newhall in initiating this project at Gede. We would like to thank Vanesa Burgos and Pablo Tierz for providing sets of analogue volcanoes and for inspiring conversations on volcanic hazard assessment. Finally, we thank Sam Engwell for comments on the initial draft, Pablo Tierz for insightful feedback and editorial handling of the manuscript, and two anonymous reviewers for their comments, all of which have greatly improved the quality of the manuscript.

Author contribution Conceptualisation: ET, SFJ, AW; Methodology: ET, SFJ; Investigation: ET, WB; Formal analysis: ET; Writing

– Original draft: ET, SFJ; Writing – Review and Editing: ET, SFJ, AW, CW, HP, NK, WB; Supervision: SFJ.

Funding This research was supported by the Ministry of Education, Singapore, under its MOE Academic Research Fund Tier 3 InVEST project (Award MOE-MOET32021-0002) and the AXA Joint Research Initiative. This work comprises EOS contribution number 644.

Data availability Additional information detailing eruptions included in the Gede plus analogues dataset and hazard model parameterisation is available in Online Resources 1–6.

Declarations

Competing interests The authors have no relevant financial or non-financial interests to disclose.

References

Alcozer-Vargas N, Reyes-Hardy MP, Esquivel A, Aguilera F (2022) A GIS-based multi-hazard assessment at the San Pedro volcano, Central Andes, Northern Chile. Front Earth Sci 10:1–25. https://doi.org/10.3389/feart.2022.897315

Andronico D, Scollo S, Cristaldi A (2015) Unexpected hazards from tephra fallouts at Mt Etna: the 23 November 2013 lava fountain. J Volcanol Geotherm Res 304:118–125. https://doi.org/10.1016/j.jvolgeores.2015.08.007

Aravena A, Cioni R, Bevilacqua A, de' Michieli Vitturi M, Esposti Ongaro T, Neri A (2020) Tree-branching based enhancement of kinetic energy models for reproducing channelization processes of pyroclastic density currents. J Geophys Res Solid Earth 125:1–20. https://doi.org/10.1029/2019JB019271

Aravena A, Bevilacqua A, Neri A, Gabellini P, Ferrés D, Escobar D, Aiuppa A, Cioni R (2023) Scenario-based probabilistic hazard assessment for explosive events at the San Salvador volcanic complex, El Salvador. J Volcanol Geotherm Res 438:1–15. https://doi.org/10.1016/j.jvolgeores.2023.107809

Arnold DWD, Biggs J, Dietterich HR, Vallejo Vargas S, Wadge G, Mothes P (2019) Lava flow morphology at an erupting andesitic stratovolcano: a satellite perspective on El Reventador, Ecuador. J Volcanol Geotherm Res 372:34–47. https://doi.org/10.1016/j.jvolgeores.2019.01.009

Aspinall WP, Woo G, Voight B, Baxter PJ (2003) Evidence-based volcanology: application to eruption crises. J Volcanol Geotherm Res 128(1–3):273–285. https://doi.org/10.1016/S0377-0273(03)00260-9

Barberi F, Bertagnini A, Landi P, Principe C (1992) A review on phreatic eruptions and their precursors. J Volcanol Geotherm Res 52:231–246. https://doi.org/10.1016/0377-0273(92)90046-G

Bartolini S, Bolós X, Martí J, Pedra ER, Planagumà L (2015) Hazard assessment at the Quaternary La Garrotxa Volcanic Field (NE Iberia). Nat Hazards 78(2):1349–1367. https://doi.org/10.1007/s11069-015-1774-y

Baxter PJ, Jenkins S, Seswandhana R, Komorowski J-C, Dunn K, Purser D, Voight B, Shelley I (2017) Human survival in volcanic eruptions: thermal injuries in pyroclastic surges, their causes, prognosis and emergency management. Burns 43:1051–1069. https://doi.org/10.1016/j.burns.2017.01.025

Bayarri MJ, Berger JO, Calder ES, Dalbey K, Lunagomez S, Patra AK, Pitman EB, Spiller ET, Wolpert RL (2009) Using statistical and computer models to quantify volcanic hazards. Technometrics 51(4):402–413. https://doi.org/10.1198/TECH.2009.08018

Bear-Crozier AN, Kartadinata N, Heriwaseso A, Nielsen O (2012) Development of python-FALL3D: a modified procedure for modelling volcanic ash dispersal in the Asia-Pacific region. Nat Hazards 64(1):821–838. https://doi.org/10.1007/s11069-012-0273-7

Bebbington MS, Stirling MW, Cronin S, Wang T, Jolly G (2018) National-level long-term eruption forecasts by expert elicitation. Bull Volcanol. https://doi.org/10.1007/s00445-018-1230-4

Bebbington MS, Jenkins SF (2019) Intra-eruption forecasting. Bull Volcanol. https://doi.org/10.1007/s00445-019-1294-9

Bebbington MS, Jenkins SF (2022) Intra-eruption forecasting using analogue volcano and eruption sets. J Geophys Res Solid Earth 127(6):1–26. https://doi.org/10.1029/2022JB024343

Becerril L, Bartolini S, Sobradelo R, Martí J, Morales JM, Galindo I (2014) Long-term volcanic hazard assessment on El Hierro (Canary Islands). Nat Hazards Earth Syst Sci 14(7):1853–1870. https://doi.org/10.5194/nhess-14-1853-2014

Belousov A, Belousova M, Krimer D, Costa F, Prambada O, Zaennudin A (2015) Volcaniclastic stratigraphy of Gede Volcano, West Java, Indonesia: how it erupted and when. J Volcanol Geotherm Res 301:238–252. https://doi.org/10.1016/j.jvolgeores.2015.05.018

Bertin D, Lindsay JM, Cronin SJ, de Silva SL, Connor CB, Caffe PJ, Grosse P, Báez W, Bustos E, Constantinescu R (2022) Probabilistic volcanic hazard assessment of the 22.5–28°S segment of the central volcanic zone of the Andes. Front Earth Sci 10:1–22. https://doi.org/10.3389/feart.2022.875439

Bertin D (2017) 3-D ballistic transport of ellipsoidal volcanic projectiles considering horizontal wind field and variable shapedependent drag coefficients. JGR Solid Earth 122:1126–1151. https://doi.org/10.1002/2016JB013320

Bevilacqua A, Aravena A, Neri A, Gutiérrez E, Escobar D, Schliz M, Aiuppa A, Cioni R (2021) Thematic vent opening probability maps and hazard assessment of small-scale pyroclastic density currents in the San Salvador volcanic complex (El Salvador) and Nejapa-Chiltepe volcanic complex (Nicaragua). Nat Hazards Earth Syst Sci 21(5):1639–1665. https://doi.org/10.5194/nhess-21-1639-2021

Biass S, Bonadonna C, Connor L et al (2016a) TephraProb: a Matlab package for probabilistic hazard assessments of tephra fallout. J Appl Volcanol 5:1–16. https://doi.org/10.1186/s13617-016-0050-5

Biass S, Bonadonna C, di Traglia F, Pistolesi M, Rosi M, Lestuzzi P (2016b) Probabilistic evaluation of the physical impact of future tephra fallout events for the Island of Vulcano, Italy. Bull Volcanol. https://doi.org/10.1007/s00445-016-1028-1

Biass S, Bonadonna C (2013) A fast GIS-based risk assessment for tephra fallout: The example of Cotopaxi volcano, Ecuador: Part I: Probabilistic hazard assessment. Natural Hazards 65:477–495. https://doi.org/10.1007/s11069-012-0378-z

Blake DM, Deligne NI, Wilson TMD, Wilson G (2017) Improving volcanic ash fragility functions through laboratory studies: example of surface transportation networks. J Appl Volcanol 6(1):1–18. https://doi.org/10.1186/s13617-017-0066-5

Blong RJ (1981) Some effects of tephra falls on buildings. In: Self S, Sparks RSJ (eds) Tephra studies. Proc. NATO ASI "tephra studies as a tool in quaternary research", Iceland, 1980. Reidel; NATO advanced study institute studies, series C 75:405–420. https://doi.org/10.1007/978-94-009-8537-7_27

Blong RJ (2003) Building damage in Rabaul, Papua New Guinea, 1994. Bull Volcanol 65(1):43–54. https://doi.org/10.1007/s00445-002-0238-x

Bonadonna C, Phillips JC, Houghton BF (2005) Modeling tephra sedimentation from a Ruapehu weak plume eruption. J Geophys Res Solid Earth. https://doi.org/10.1029/2004JB003515

Burgos V, Jenkins SF, Bono Troncoso L, Perales Moya CV, Bebbington M, Newhall C, Amigo A, Prada Alonso J, Taisne B (2023) Identifying analogues for data-limited volcanoes using hierarchical clustering and expert knowledge: a case study of Melimoyu (Chile). Front Earth Sci 11:1144386. https://doi.org/10.3389/feart.2023.1144386

Calvari S, Pinkerton H (2002) Instabilities in the summit region of Mount Etna during the 1999 eruption. Bull Volcanol 63:526–535. https://doi.org/10.1007/s004450100171

Carrara A, Pinel V, Bascou P, Chaljub E, de la Cruz-Reyna S (2019) Post-emplacement dynamics of andesitic lava flows at Volcán de Colima, Mexico, revealed by radar and optical remote sensing data. J Volcanol Geotherm Res 381:1–15. https://doi.org/10.1016/j.jvolgeores.2019.05.019

Clarke B, Tierz P, Calder E, Yirgu G (2020) Probabilistic volcanic hazard assessment for pyroclastic density currents from pumice cone eruptions at Aluto volcano. Ethiopia Front Earth Sci 8(August):1–19. https://doi.org/10.3389/feart.2020.00348

Connor LJ, Connor CB, Meliksetian K, Savov I (2012) Probabilistic approach to modeling lava flow inundation: a lava flow hazard assessment for a nuclear facility in Armenia. J Appl Volcanol 1(1):1–19. https://doi.org/10.1186/2191-5040-1-3

Constantinescu R, González-Zuccolotto K, Ferrés D, Sieron K, Siebe C, Connor C, Capra L, Tonini R (2022) Probabilistic volcanic hazard assessment at an active but under-monitored volcano: Ceboruco, Mexico. J Appl Volcanol. https://doi.org/10.1186/s13617-022-00119-w

Dalbey K (2009) Predictive simulation and model based hazard maps of geophysical mass flows. PhD thesis, State University of New York at Buffalo, USA

Dellino P, Dioguardi F, Isaia R, Sulpizio R, Mele D (2021) The impact of pyroclastic density currents duration on humans: the case of the AD 79 eruption of Vesuvius. Sci Rep 11(1):4959

Degruyter W, Bonadonna C (2012) Improving on mass flow rate estimates of volcanic eruptions. Geophys Res Lett 39(16):1–6. https://doi.org/10.1029/2012GL052566

de Castro, F (2025). fitmethis (https://www.mathworks.com/matlabcentral/fileexchange/40167-fitmethis), MATLAB Central File Exchange. Retrieved September 27, 2024.

Fitzgerald RH, Tsunematsu K, Kennedy BM, Breard ECP, Lube G, Wilson TM, Jolly AD, Pawson J, Rosenberg MD, Cronin SJ (2014) The application of a calibrated 3D ballistic trajectory model to ballistic hazard assessments at Upper Te Maari, Tongariro. J Volcanol Geotherm Res 286:248–262. https://doi.org/10.1016/j.jvolgeores.2014.04.006

Folch A, Mingari L, Osores MS, Collini E (2014) Modeling volcanic ash resuspension - application to the 14–18 october 2011 outbreak episode in central Patagonia, Argentina. Nat Hazards Earth Syst Sci 14(1):119–133. https://doi.org/10.5194/nhess-14-119-2014

Folch A, Mingari L, Gutierrez N, Hanzich M, Macedonio G, Costa A (2020) FALL3D-8.0: a computational model for atmospheric transport and deposition of particles, aerosols and radionuclides – part 1: model physics and numerics. Geosci Model Dev 13(3):1431–1458. https://doi.org/10.5194/gmd-13-1431-2020

Gallant E, Richardson J, Connor C, Wetmore P, Connor L (2018) A new approach to probabilistic lava flow hazard assessments, applied to the Idaho National Laboratory, eastern Snake River Plain, Idaho, USA. Geology 46(10):895–898. https://doi.org/10.1130/G45123.1

Geospatial Information Agency (2018) Geospatial Information Agency, DEMNAS, http://tides.big.go.id/DEMNAS/

Grosse P, Euillades PA, Euillades LD, Vries B, van W de (2014) A global database of composite volcano morphometry. Bulletin of Volcanology 76, 1–16. https://doi.org/10.1007/s00445-013-0784-4

Gjerløw E, Höskuldsson Á, Bartolini S, Biass S, Mossoux S, Gilbert J, Pedersen RB, Martí J (2022) The volcanic hazards of Jan Mayen Island (North-Atlantic). Front Earth Sci 10:1–19. https://doi.org/10.3389/feart.2022.730734

Global Volcanism Program (1976) Report on Karangetang (Indonesia) (Squires D, ed.). Nat Sci Event Bull 1:14. Smithsonian Institution. https://doi.org/10.5479/si.GVP.NSEB197611-267020

Hadisantono RD, Abdurachman A, Martono A, Sumpena AD, Wahyu S, Santoso MS (2008) Volcanic hazard map of gede volcano, west java province, 1:50,000. Centre of volcanology and geological hazard mitigation, Geological Agency Indonesia, Jakarta, Indonesia, Map

Handley HK, Macpherson CG, Davidson JP (2010) Geochemical and Sr-O isotopic constraints on magmatic differentiation at Gede Volcanic Complex, West Java, Indonesia. Contrib Mineral Petrol 159(6):885–908. https://doi.org/10.1007/s00410-009-0460-z

Harnett CE, Thomas ME, Calder ES, Ebmeier SK, Telford A, Murphy W, Neuberg J (2019) Presentation and analysis of a worldwide database for lava dome collapse events: the Global archive of dome instabilities (GLADIS). Bull Volcanol 81(3):1–17. https://doi.org/10.1007/s00445-019-1276-y

Hayes JL, Wilson TM, Deligne NI, Lindsay JM, Leonard GS, Tsang SWR, Fitzgerald RH (2020) Developing a suite of multihazard volcanic eruption scenarios using an interdisciplinary approach. J Volcanol Geotherm Res 392:1–19. https://doi.org/10.1016/j.jvolgeores.2019.106763

Hayes JL, Jenkins SF, Joffrain M (2022) Large Uncertainties Are Pervasive in Long-Term Frequency-Magnitude Relationships for Volcanoes in Southeast Asia. Front Earth Sci 10:1–19. https://doi.org/10.3389/feart.2022.895756

Hersbach H, Bell B, Berrisford P, Hirahara S, Horányi A, Muñoz-Sabater J, Nicolas J, Peubey C, Radu R, Schepers D, Simmons A, Soci C, Abdalla S, Abellan X, Balsamo G, Bechtold P, Biavati G, Bidlot J, Bonavita M, Thépaut JN (2020) The ERA5 global reanalysis. Q J R Meteorol Soc 146(730):1999–2049. https://doi.org/10.1002/qj.3803

Heim A (1932) Bergsturz und Menschenleben. Fretz und Wasmuth, Zurich, Switzerland, p 218

Hidayat D, Basuki A, Nurrokhman N, Kristianto K, Taisne B (2019) Volcanic structure under Gede, West Java, Indonesia, results from three-dimensional local earthquake tomography and small long-period earthquake analysis. In: EGU General Assembly, Vienna, Austria

Hincks TK, Komorowski J-C, Sparks SR, Aspinall WP (2014) Retrospective analysis of uncertain eruption precursors at La Soufrière volcano, Guadeloupe, 1975–77: volcanic hazard assessment using a Bayesian belief network approach. J Appl Volcanol 3:1–26

Jenkins SF, Komorowski J-C, Baxter PJ, Spence R, Picquout A, Lavigne F, Surono (2013) The Merapi 2010 eruption: an interdisciplinary impact assessment methodology for studying pyroclastic density current dynamics. J Volcanol Geotherm Res 261, 316–329. https://doi.org/10.1016/j.jvolgeores.2013.02.012

Jenkins SF, Spence RJS, Fonseca JFBD, Solidum RU, Wilson TM (2014) Volcanic risk assessment: quantifying physical

vulnerability in the built environment. J Volcanol Geotherm Res 276:105–120. https://doi.org/10.1016/j.jvolgeores.2014.03.002

Jenkins SF, Wilson T, Magill C, Miller V, Stewart C, Blong RJ, Marzocchi W, Boulton M, Bonadonna C, Costa A (2015) Volcanic ash fall hazard and risk. In: Global Volcanic Hazards and Risk. Cambridge University Press, pp 173–221. https://doi.org/10.1017/CBO9781316276273.005

Jenkins SF, Biass S, Williams GT, Hayes JL, Tennant E, Yang Q, Burgos V, Meredith ES, Lerner GA, Syarifuddin M, Verolino A (2022) Evaluating and ranking Southeast Asia's exposure to explosive volcanic hazards. Nat Hazards Earth Syst Sci 22:1233–1265. https://doi.org/10.5194/nhess-22-1233-2022

Jenkins SF, Mee K, Engwell SL, Loughlin SC, Faria BVE, Yirgu G, Bekele Y, Lewi E, Vye-Brown C, Fraser SA, Day SJ, Lark RM, Huyck C, Crummy J (2024a) Assessing volcanic hazard and exposure in a data poor context: case study for Ethiopia, Kenya, and Cabo Verde. Prog Disaster Sci 100350:1–19. https://doi.org/10.1016/j.pdisas.2024.100350

Jenkins SF, McSporran A, Wilson TM, Stewart C, Leonard G, Cevuard S, Garaebiti E (2024b) Tephra fall impacts to buildings: the 2017–2018 Manaro Voui eruption, Vanuatu. Front Earth Sci 12:1–19. https://doi.org/10.3389/feart.2024.1392098

Jiménez D, Becerril L, Bartolini S, Escobar D, Martí J (2020) Making a qualitative volcanic-hazards map by combining simulated scenarios: an example for San Miguel Volcano (El Salvador). J Volcanol Geotherm Res 395:1–9. https://doi.org/10.1016/j.jvolgeores.2020.106837

Krimer D (2016) Unraveling the evolution, dynamics and time-scales of magmatic processes below the volcano, West-Java, Indonesia. PhD thesis, Nanyang Technological University, Singapore. https://doi.org/10.32657/10356/68520

Lerner GA, Jenkins SF, Charbonnier SJ, Komorowski JC, Baxter PJ (2022) The hazards of unconfined pyroclastic density currents: a new synthesis and classification according to their deposits, dynamics, and thermal and impact characteristics. J Volcanol Geotherm Res 421:1–20. https://doi.org/10.1016/j.jvolgeores.2021.107429

Lindsay JM, Charlton D, Clive MAT, Bertin D, Ogburn S, Wright H, Ewert J, Calder ES, Steinke B (2023) The diversity of volcanic hazard maps around the world: insights from map makers. J Appl Volcanol 12(1):1–26. https://doi.org/10.1186/s13617-023-00134-5

Lombardi AM, del Gaudio P, Guo Z, Zhang M, Liu G, Sepe V, Liu J, Ventura G (2020) Scenario-based pyroclastic density current invasion maps at poorly known volcanoes: a case study from Changbaishan (China/North Korea). Appl Sci (Switzerland) 10(7):1–19. https://doi.org/10.3390/app10072622

Loughlin SC, Vye-Brown C, Sparks RSJ, Brown B, Barclay J, Calder E, Cottrell E, Jolly G, Komorowski J-C, Mandeville C, Newhall CG, Palma JL, Potter S, Valentine G (2015) An introduction to global volcanic hazard and risk. In: Loughlin SC, Sparks S, Brown SK, Jenkins SF, Vye-Brown C (eds) Global Volcanic Hazards and Risk. Cambridge University Press, pp 1–80

Mastin LG, Guffanti M, Ewert JW, Spiegel J (2009) Preliminary Spreadsheet of Eruption Source Parameters for Volcanoes of the World. At: http://pubs.usgs.gov/of/2009/1133/. Last Accessed: 15 July 2024

Martí J, Becerril L, Rodríguez A (2022) How long-term hazard assessment may help to anticipate volcanic eruptions: the case of La Palma eruption 2021 (Canary Islands). J Volcanol Geotherm Res 431:1–15. https://doi.org/10.1016/j.jvolgeores.2022.107669

Marzocchi W, Sandri L, Gasparini P, Newhall C, Boschi E (2004) Quantifying probabilities of volcanic events: the example of volcanic hazard at Mount Vesuvius. J Geophys Res Solid Earth. https://doi.org/10.1029/2004JB003155

Marzocchi W, Sandri L, Selva J (2008) BET_EF: a probabilistic tool for long- and short-term eruption forecasting. Bull Volcanol 70(5):623–632. https://doi.org/10.1007/s00445-007-0157-y

Marzocchi W, Sandri L, Selva J (2010) BET_VH: a probabilistic tool for long-term volcanic hazard assessment. Bull Volcanol 72(6):705–716. https://doi.org/10.1007/s00445-010-0357-8

Marzocchi W, Bebbington MS (2012) Probabilistic eruption forecasting at short and long time scales. Bull Volcanol 74(8):1777–1805. https://doi.org/10.1007/s00445-012-0633-x

Mead S, Procter J, Bebbington M, Rodriguez-Gomez C (2022) Probabilistic volcanic hazard assessment for national park infrastructure proximal to Taranaki volcano (New Zealand). Front Earth Sci 10:1–17. https://doi.org/10.3389/feart.2022.832531

Natuurk Tjidschrift von Nederlandische Indie (NTNI), Pt. 3, 1852, pp 337–338. (In Dutch)

Natuurk Tjidschrift von Nederlandische Indie (NTNI), Pt 18, 1859, p 295. (In Dutch)

Natuurk Tjidschrift von Nederlandische Indie (NTNI), Pt. 32 1871. pp 251–259. (In Dutch)

Natuurk Tjidschrift von Nederlandische Indie (NTNI), Pt. 46:1, 1886. pp 269–287. (In Dutch)

Natuurk Tjidschrift von Nederlandische Indie (NTNI), Pt 47:1, 1887, pp 528–559. (In Dutch)

Natuurk Tjidschrift von Nederlandische Indie (NTNI), Pt 48, 1889, pp 199–209. (In Dutch)

Natuurk Tjidschrift von Nederlandische Indie (NTNI), Pt 49, 1890, pp 11–159. (In Dutch)

Natuurk Tjidschrift von Nederlandische Indie (NTNI), 1891. Pt 50, pp 166-197. (In Dutch)

Natuurk Tjidschrift von Nederlandische Indie (NTNI), Pt. 60:2, 1900, pp 157–218. (In Dutch)

Natuurk Tjidschrift von Nederlandische Indie (NTNI), 1902. pt 61, pp 195–249. (In Dutch)

Natuurk Tjidschrift von Nederlandische Indie (NTNI), Pt 84:1, 1924, pp 15–86. (In Dutch)

Nurwulan RL (2016) Heritage of Gede Pangrango mountain: the potential economical aspect in Cipanas Cianjur Jawa Barat. AKURAT, Jurnal Ilmiah Akuntansi 7(1):53–55

Ogburn SE (2012) Flowdat: Mass flow database v2.2. On Vhub at: https://vhub.org/groups/massflowdatabase

Ogburn SE, Calder ES (2017) The relative effectiveness of empirical and physical models for simulating the dense undercurrent of pyroclastic flows under different emplacement conditions. Front Earth Sci 5(83):1–26. https://doi.org/10.3389/feart.2017.00083

Osman S, Rossi E, Bonadonna C, Frischknecht C, Andronico D, Cioni R, Scollo S (2019) Exposure-based risk assessment and emergency management associated with the fallout of large clasts at Mount Etna. Nat Hazards Earth Syst Sci 19(3):589–610. https://doi.org/10.5194/nhess-19-589-2019

Patra AK, Bauer AC, Nichita CC, Pitman EB, Sheridan MF, Bursik M, Rupp B, Webber A, Stinton AJ, Namikawa LM, Renschler CS (2005) Parallel adaptive numerical simulation of dry avalanches over natural terrain. J Volcanol Geotherm Res 139(1–2):1–21. https://doi.org/10.1016/j.jvolgeores.2004.06.014

Pesaresi M, Panagiotis P (2023) GHS-BUILT-C R2023A - GHS Settlement Characteristics, derived from Sentinel2 composite (2018) and other GHS R2023A data. European Commission, Joint Research Centre (JRC). PID: http://data.europa.eu/89h/3c60ddf6-0586-4190-854b-f6aa0edc2a30. https://doi.org/10.2905/3C60DDF6-0586-4190-854B-F6AA0EDC2A30

Petroeschevsky WA (1952) The volcanic activity in Indonesia during the period 1942–1948. Berita Gunung Berapi 1:17–30; 3–4:931.

Procter JN, Cronin SJ, Platz T, Patra A, Dalbey K, Sheridan M, Neall V (2009) Mapping block-and-ash flow hazards based on Titan

2D simulations: a case study from Mt. Taranaki, NZ. Nat Hazards 53(3):483–501. https://doi.org/10.1007/s11069-009-9440-x

Reyes-Hardy MP, Aguilera Barraza F, Sepúlveda Birke JP, Esquivel Cáceres A, Inostroza Pizarro M (2021) GIS-based volcanic hazards, vulnerability and risks assessment of the Guallatiri Volcano, Arica y Parinacota Region. Chile J South Am Earth Sci 109(103262):1–21. https://doi.org/10.1016/j.jsames.2021.103262

Rossi E, Bonadonna C, Degruyter W (2019) A new strategy for the estimation of plume height from clast dispersal in various atmospheric and eruptive conditions. Earth Planet Sci Lett 505:1–12. https://doi.org/10.1016/j.epsl.2018.10.007

Rupp B, Bursik M, Namikawa L, Webb A, Patra AK, Saucedo R, Macías JL, Renschler C (2006) Computational modeling of the 1991 block and ash flows at Colima Volcano, México. Spec Pap Geol Soc Am 402:237–252. https://doi.org/10.1130/2006.2402

Sandri L, Jolly G, Lindsay J, Howe T, Marzocchi W (2012) Combining long- and short-term probabilistic volcanic hazard assessment with cost-benefit analysis to support decision making in a volcanic crisis from the Auckland Volcanic Field, New Zealand. Bull Volcanol 74:705–723. https://doi.org/10.1007/s00445-011-0556-y

Sandri L, Thouret JC, Constantinescu R, Biass S, Tonini R (2014) Long-term multi-hazard assessment for El Misti volcano (Peru). Bull Volcanol 76:1–26. https://doi.org/10.1007/s00445-013-0771-9

Sandri L, Tierz P, Costa A, Marzocchi W (2018) Probabilistic hazard from pyroclastic density currents in the Neapolitan area (Southern Italy). J Geophys Res Solid Earth 123:3474–3500. https://doi.org/10.1002/2017JB014890

Siebert L, Simkin T, Kimberly P (2011) Volcanoes of the world, 3rd ed. Smithsonian Institution, Washington, D.C. Berkeley ; University of California Press

Schiavina M, Freire S, Carioli A, MacManus K (2023) GHS-POP R2023A - GHS population grid multitemporal (1975–2030). Eur Comm Joint Res Centre (JRC). PID: http://data.europa.eu/89h/2ff68a52-5b5b-4a22-8f40-c41da8332cfe. https://doi.org/10.2905/2FF68A52-5B5B-4A22-8F40-C41DA8332CFE

Sheridan MF, Stinton AJ, Patra A, Pitman EB, Bauer A, Nichita CC (2005) Evaluating Titan2D mass-flow model using the 1963 Little Tahoma Peak avalanches, Mount Rainier, Washington. J Volcanol Geotherm Res 139:89–102. https://doi.org/10.1016/j.jvolgeores.2004.06.011

Small C, Naumann T (2001) The global distribution of human population and recent volcanism. Global Environmental Change Part B: Environmental Hazards 3(3–4):93–109. https://doi.org/10.1016/S1464-2867(02)00002-5

Sobradelo R, Bartolini S, Martí J (2014) HASSET: a probability event tree tool to evaluate future volcanic scenarios using Bayesian inference. Bull Volcanol 76:1–15. https://doi.org/10.1007/s00445-013-0770-x

Spiller ET, Bayarri MJ, Berger JO, Calder ES, Patra AK, Pitman EB, Wolpert RL (2014) Automating emulator construction for geophysical hazard maps. SIAM ASA J Uncertain Quantif 2:126–152. https://doi.org/10.1137/120899285

Stinton AJ, Sheridan MF, Patra A, Dalbey K, Namikawa N (2004) Incorporation of variable bed friction into Titan2D mass-flow model: application to Little Tahoma Peak avalanche (Washington). Acta Vulcanol 16(1–2):153–164. https://doi.org/10.1400/19102

Stix J, de Moor JM (2018) Understanding and forecasting phreatic eruptions driven by magmatic degassing. Earth Planets Space 70(1):1–19. https://doi.org/10.1186/s40623-018-0855-z

Sulpizio R, Capra L, Sarocchi D, Saucedo R, Gavilanes-Ruiz JC, Varley NR (2010) Predicting the block-and-ash flow inundation areas at Volcán de Colima (Colima, Mexico) based on the present day (February 2010) status. J Volcanol Geotherm Res 193:49–66. https://doi.org/10.1016/j.jvolgeores.2010.03.007

Supendi P, Nugraha AD, Puspito NT, Widiyantoro S, Daryono D (2018) Identification of active faults in West Java, Indonesia, based on earthquake hypocenter determination, relocation, and focal mechanism analysis. Geosci Lett 5(1):1–10. https://doi.org/10.1186/s40562-018-0130-y

Tang FHM, Nguyen TH, Conchedda G, Casse L, Tubiello FN, Maggi F (2024) CROPGRIDS: a global geo-referenced dataset of 173 crops. Sci Data 11(1):1–14. https://doi.org/10.1038/s41597-024-03247-7

Tadini A, Cerminara M, Paris R, Neri A, Sparks RSJ, Vougioukalakis G, Koutroulli A, Calusi B (2025) Scenario-based tsunami hazard assessment at Kolumbo submarine volcano. Bull Volcanol 87:52. https://doi.org/10.1007/s00445-025-01837-w

Tennant E, Jenkins SF, Winson A, Widiwijayanti C, Gunawan H, Haerani N, Kartadinata N, Banggur W, Triastuti H (2021) Reconstructing eruptions at a data limited volcano: a case study at Gede (West Java). J Volcanol Geotherm Res 418:107325. https://doi.org/10.1016/j.jvolgeores.2021.107325

Tennant E, Jenkins SF, Biass S (2023) FlowDIR: a MATLAB tool for rapidly and probabilistically forecasting the travel directions of volcanic flows. J Appl Volcanol 12(136):1–19. https://doi.org/10.1186/s13617-023-00136-3

Tennant E, Jenkins SF, Miller V, Robertson R, Wen B, Yun SH, Taisne B (2024) Automating tephra fall building damage assessment using deep learning. Nat Hazards Earth Syst Sci 24:4585–4608. https://doi.org/10.5194/nhess-24-4585-2024

Tierz P, Sandri L, Costa A, Zaccarelli L, di Vito MA, Sulpizio R, Marzocchi W (2016) Suitability of energy cone for probabilistic volcanic hazard assessment: validation tests at Somma-Vesuvius and Campi Flegrei (Italy). Bull Volcanol 78(11):79–93. https://doi.org/10.1007/s00445-016-1073-9

Tierz P, Woodhouse MJ, Phillips JC, Sandri L, Selva J, Marzocchi W, Odbert HM (2017) A framework for probabilistic multi-hazard assessment of rain-triggered lahars using Bayesian belief networks. Front Earth Sci 5:73. https://doi.org/10.3389/feart.2017.00073

Tierz P, Stefanescu ER, Sandri L, Sulpizio R, Valentine GA, Marzocchi W, Patra AK (2018) Towards quantitative volcanic risk of pyroclastic density currents: probabilistic hazard curves and maps around Somma-Vesuvius (Italy). J Geophys Res Solid Earth 123:6299–6317. https://doi.org/10.1029/2017jb015383

Tierz P, Loughlin SC, Calder ES (2019) VOLCANS: an objective, structured and reproducible method for identifying sets of analogue volcanoes. Bull Volcanol 81(1336):1–16. https://doi.org/10.1007/s00445-019-1336-3

Tierz P (2020) Long-term probabilistic volcanic hazard assessment using open and non-open data: observations and current issues. Front Earth Sci 8:257. https://doi.org/10.3389/feart.2020.00257

Tierz et al (2021) PyVOLCANS: A Python package to flexibly explore similarities and differences between volcanic systems. J Open Source Softw 6(68):3649. https://doi.org/10.21105/joss.03649

Tierz P, Spiller ET, Clarke BA, Dessalegn F, Bekele Y, Lewi E, Yirgu G, Wolpert RL, Loughlin SC, Calder ES (2024) Topographic controls on pyroclastic density current hazard at Aluto Volcano (Ethiopia) identified using a novel zero-censored Gaussian process emulator. J Geophys Res Solid Earth. https://doi.org/10.1029/2023JB028645

Tsang SWR, Lindsay JM (2020) Lava flow crises in inhabited areas part I: lessons learned and research gaps related to effusive, basaltic eruptions. J Appl Volcanol 9:1–26. https://doi.org/10.1186/s13617-020-00096-y

United Nations International Strategy for Disaster Reduction (UNISDR), (2005) Hyogo Framework for Action 2005–2015: Building the resilience of nations and communities to disasters. United Nations International Strategy for Disaster Reduction, Geneva, Switzerland

United Nations International Strategy for Disaster Reduction (2015) Sendai framework for disaster risk reduction 2015–2030. United Nations Office for Disaster Risk Reduction, Geneva, Switzerland

Valentine GA (1998) Damage to structures by pyroclastic flows and surges, inferred from nuclear weapons effects. J Volcanol Geotherm Res 87, 117–140. https://doi.org/10.1016/S0377-0273(98)00094-8

Vázquez R, Macías JL, Arce JL, Cisneros G, Saucedo R (2019) Numerical simulation of block-and-ash flows for different eruptive scenarios of the Tacaná Volcanic Complex, México-Guatemala. J Volcanol Geotherm Res 373:36–50. https://doi.org/10.1016/j.jvolgeores.2019.01.026

Verolino A, Jenkins SF, Sieh K, Herrin JS, Schonwalder-Angel D, Sihavong V, Oh JH (2022) Assessing volcanic hazard and exposure to lava flows at remote volcanic fields: a case study from the Bolaven Volcanic Field. Laos J Appl Volcanol 11(116):1–15. https://doi.org/10.1186/s13617-022-00116-z

Warwick R, Williams-Jones G, Kelman M, Witter J (2022) A scenario-based volcanic hazard assessment for the mount meager volcanic complex. British Columbia J Appl Volcanol 11(1):1–22. https://doi.org/10.1186/s13617-022-00114-1

Weir AM, Mead S, Bebbington MS, Wilson TM, Beaven S, Gordon T, Campbell-Smart C (2022) A modular framework for the development of multi-hazard, multi-phase volcanic eruption scenario suites. J Volcanol Geotherm Res 427:1–19. https://doi.org/10.1016/j.jvolgeores.2022.107557

Widiwijayanti C, Hidayat D, Voight B, Patra A, Pitman EB (2007) Modelling dome-collapse pyroclastic flows for crisis assessments on Montserrat with TITAN2D. Cities on Volcanoes 5 Conference, Shimabara, Japan, 11-P-34.

Winson AEG (2016) Multiparametric Quantification of Volcanic Hazards for Eruption Forecasting and Communication. PhD thesis, Nanyang Technological University, Singapore

Whelley PL, Newhall CG, Bradley KE (2015) The frequency of explosive volcanic eruptions in Southeast Asia. Bull Volcanol 77(1):1–11. https://doi.org/10.1007/s00445-014-0893-8

Widiwijayanti C, Voight B, Hidayat D, Schilling SP (2009) Objective rapid delineation of areas at risk from block-and-ash pyroclastic flows and surges. Bull Volcanol 71(6):687–703. https://doi.org/10.1007/s00445-008-0254-6

Williams GT, Kennedy BM, Wilson TM, Fitzgerald RH, Tsunematsu K, Teissier A (2017) Buildings vs. ballistics: Quantifying the vulnerability of buildings to volcanic ballistic impacts using field studies and pneumatic cannon experiments. J Volcanol Geotherm Res 343, 171–180. https://doi.org/10.1016/j.jvolgeores.2017.06.026

Williams GT, Kennedy BM, Lallemant D, Wilson TM, Allen N, Scott A, Jenkins SF (2019) Tephra cushioning of ballistic impacts: quantifying building vulnerability through pneumatic cannon experiments and multiple fragility curve fitting approaches. J Volcanol Geotherm Res 388:106711. https://doi.org/10.1016/j.jvolgeores.2019.106711

Williams GT, Jenkins SF, Biass S, Wibowo HE, Harijoko A (2020) Remotely assessing tephra fall building damage and vulnerability: Kelud Volcano, Indonesia. J Appl Volcanol 9(1):10. https://doi.org/10.1186/s13617-020-00100-5

Wilson L, Sparks RSJ, Huang TC, Watkins ND (1978) The control of volcanic column heights by eruption energetics and dynamics. J Geophys Res 83:1829–1836

World Population Review (2024) https://worldpopulationreview.com/. Accessed 1 Nov 2024

Yoganandan N, Pintar FA, Sances JA, Walsh PR, Ewing CL, Thomas DJ, Snyder RG (1995) Biomechanics of skull fracture. J Neurotrauma 12:659–668

Zuccaro G, Cacace F, Spence RJS, Baxter PJ (2008) Impact of explosive eruption scenarios at Vesuvius. J Volcanol Geotherm Res 178:416–453. https://doi.org/10.1016/j.jvolgeores.2008.01.005

Zuccaro G, De Gregorio D (2013) Time and space dependency in impact damage evaluation of a sub-Plinian eruption at Mount Vesuvius. Nat Hazards 68:1399–1423. https://doi.org/10.1007/s11069-013-0571-8